Available online at www.sciencedirect.com
SCIENCE DIRECT®
Estuarine, Coastal and Shelf Science 61 (2004) 403–424
ESTUARINE COASTAL AND SHELF SCIENCE
www.elsevier.com/locate/ECSS

Bio-optical model for Chesapeake Bay and the Middle Atlantic Bight

Andrea Magnuson[a], Lawrence W. Harding Jr.[a,b,*], Michael E. Mallonee[a], Jason E. Adolf[a]

[a]*Horn Point Laboratory, University of Maryland, Center for Environmental Science, Box 775, Cambridge, MD 21613, USA*
[b]*Maryland Sea Grant College, University of Maryland, 4321 Hartwick Road, Suite 300, College Park, MD 20740, USA*

Received 29 October 2003; accepted 9 June 2004

Abstract

Retrievals of bio-optical properties from satellite measurements in Case 2 waters depend on algorithms that account for multiple constituents affecting spectral quality of the upwelling light flux. Semi-analytical (SA) models are suitable for this purpose, but must be parameterized with in situ data, particularly in estuarine and coastal waters. We examined spatial and temporal variability of bio-optical properties in Chesapeake Bay and the adjacent Middle Atlantic Bight (CB/MAB) to parameterize and validate the Garver/Siegel/Maritorena (GSM01) model. Several years (1996–2002) of data on inherent and apparent optical properties confirmed high scattering and strong absorption by dissolved and particulate components that did not co-vary. These data, consisting of the chlorophyll (chl *a*)-normalized phytoplankton absorption coefficient, $a^*_{ph}(\lambda)$, and the spectral slope of absorption due to dissolved and detrital materials, S_{cdm}, were used to optimize model parameters of GSM01 and produce a version of the model tuned for CB/MAB we have designated GSM01-CB. Performance of GSM01-CB was measured against the globally optimized version of GSM01 and the empirical algorithm, OC4v.4, using both in situ and satellite-derived radiances from the *S*ea-viewing *W*ide *F*ield-of-view *S*ensor (SeaWiFS) as inputs to the model. GSM01-CB outperformed OC4v.4 in retrieving chl *a* in CB, and both SA models outperformed OC4v.4 in MAB. GSM01 and GSM01-CB also returned reasonable estimates of other bio-optical products, including the absorption coefficient for dissolved and detrital materials, $a_{cdm}(443)$, and the particulate backscatter coefficient, $b_{bp}(443)$. We present alternatives to the parameterization of GSM01-CB to account for interannual variability of $a^*_{ph}(\lambda)$ in CB using empirical relationships with key variables that regulate phytoplankton dynamics in the estuary (i.e., freshwater flow and nutrient loading), and to include regional gradients of S_{cdm} in MAB.

Keywords: bio-optical modeling; remote sensing; Case 2 algorithms

1. Introduction

Bio-optical properties of estuarine and coastal waters, including Chesapeake Bay (CB) and the Middle Atlantic Bight (MAB), are strongly influenced by high concentrations of phytoplankton, dissolved organic material, and suspended sediments (Harding et al., submitted for publication). These 'Case 2' waters are defined by a mix of bio-optically active components that do not co-vary, complicating the accurate retrieval of chlorophyll (chl *a*) using remote sensing of ocean color from aircraft and satellite sensors. Satellite estimates of chl *a* heretofore have been based on empirical algorithms, such as OC4v.4 that is used to estimate chl *a* from

* Corresponding author.
E-mail address: larry@hpl.umces.edu (L.W. Harding Jr.).

0272-7714/$ - see front matter © 2004 Elsevier Ltd. All rights reserved.
doi:10.1016/j.ecss.2004.06.020

*S*ea-viewing *W*ide *F*ield-of-view *S*ensor (SeaWiFS) data (O'Reilly et al., 1998). Empirical algorithms are based on statistical relationships between chl *a* and light emanating from the ocean, normalized water-leaving radiance, L_{WN}, or remote sensing reflectance, R_{RS}. The presence of high concentrations of chromophoric dissolved organic matter (CDOM) and suspended particulate matter (SPM) limit the accuracy of empirical algorithms (Gordon and Morel, 1983; Jorgensen, 1999). Semi-analytical (SA) models relate R_{RS} to the multiple constituents of the water column that control absorption and scattering of light, including absorptions due to phytoplankton, a_{ph}, CDOM, a_{cdom}, and non-pigmented particulate material, a_d, and backscattering due to particles, b_{bp} (Gordon et al., 1988; Morel, 1988; Roesler and Perry, 1995; Garver and Siegel, 1997; Carder et al., 1999). These models have the potential to improve estimates of chl *a* for estuarine and coastal ecosystems when appropriately tuned for the bio-optical properties in the region of interest. In addition to chl *a*, SA models return estimates of absorption due to dissolved and non-pigmented particulate matter and backscattering that have applications in the coastal zone (see Parslow et al., 2000).

Detailed in situ measurements of bio-optical properties of CB/MAB have been conducted in the past decade to support a variety of missions, including SeaWiFS, the Sensor Inter-comparison and Merger for Biological and Interdisciplinary Oceanic Studies (SIMBIOS), and the Moderate Resolution Imaging Spectrometer (MODIS). These measurements include inherent optical properties (IOPs) and apparent optical properties (AOPs) in CB/MAB that now span nearly a decade. We are currently positioned to use these data to tune a SA model for the CB/MAB region. SA models developed by Carder et al. (2003) and Maritorena et al. (2002) have been incorporated into data processing for MODIS and SeaWiFS, respectively, to retrieve chl *a* and other products for the global ocean. The model described in Maritorena et al. (2002), termed the Garver-Siegel-Maritorena (GSM01) model, was selected because modifications to the model could be made in the source code of the SeaWiFS Data Analysis System (SeaDAS), allowing us to test modifications to the model using satellite data. The native version of GSM01 employs a fixed set of model parameters derived using a 'statistical optimization procedure' to maximize performance for the global ocean. The parameterization was based on in situ bio-optical measurements for Case 1 waters from the SeaWiFS Bio-Optical Algorithm Mini-Workshop (SeaBAM) data set. In contrast to Case 1 waters, CB/MAB waters are strongly affected by inputs of CDOM and SPM from the Susquehanna River and other tributaries, resulting in strong spatial gradients of a_{cdom} and a_d from CB proper to the shelf (Harding et al., submitted for publication). Seasonal and interannual variability of freshwater flow drives a well-documented annual cycle of species composition, characterized by the predominance of diatoms in spring and flagellates in summer, that affect the absorption properties of phytoplankton. Ideally, this seasonal and regional variability of bio-optical properties should be included in a regionally tuned SA model.

The goal of this research was to improve retrievals of chl *a*, as well as primary productivity (PP) that depends on accurate estimates of biomass (cf. Harding et al., 2002), by developing a regional version of GSM01 parameterized and validated with bio-optical data for CB/MAB. We addressed this goal in several steps: (1) an extensive set of bio-optical data for CB/MAB was used to quantify the magnitude and variability of key model inputs on seasonal and regional bases, principally a_{ph} normalized to chl *a*, $a^*_{ph}(\lambda)$, and the spectral slope of colored dissolved and detrital material, S_{cdm}; (2) the regionally and seasonally tuned parameters were applied to GSM01, producing a modified version of the model that we termed GSM01-CB; (3) chl *a* retrievals from GSM01-CB using in situ measurements of R_{RS} were compared to those from the native form, GSM01, and to retrievals from the empirical SeaWiFS algorithm, OC4v.4; (4) GSM01-CB was incorporated into the SeaDAS code to compare the output of the various models for SeaWiFS radiance observations; and (5) we identified empirical relationships between model parameters and other variables that could be incorporated into a bio-optical model to better resolve variability within regions and seasons not addressed in parameterization of GSM01-CB.

2. Methods

2.1. Model development

The GSM01 reflectance inversion model described by Maritorena et al. (2002) is based on the relationship of L_{WN} and absorption, *a*, and backscattering, b_b, coefficients, as presented by Gordon et al. (1988):

$$L_{WN}(\lambda) = \frac{tF_0(\lambda)}{n_w^2} \sum_{i=1}^{2} \times g_i \left(\frac{b_{bw}(\lambda) + b_{bp}(\lambda)}{b_{bw}(\lambda) + b_{bp}(\lambda) + a_w(\lambda) + a_{ph}(\lambda) + a_{cdm}(\lambda)} \right)^i \quad (1)$$

where λ refers to SeaWiFS wavebands (412, 443, 490, 555, 670 nm), *t* is the sea–air transmission factor, $F_0(\lambda)$ is extraterrestrial solar irradiance, n_w is the index of refraction of water, and g_i terms are modeled coefficients derived from Monte Carlo simulations that describe the

effects of sun elevation and atmospheric conditions on the upwelling light field (Morel and Gentili, 1991, 1993). a is expressed as the linear sum of absorption by seawater, $a_w(\lambda)$, phytoplankton, $a_{ph}(\lambda)$, the combined absorption of dissolved and particulate material, $a_{cdm}(\lambda)$, and b_b is the sum of backscatter due to seawater, $b_{bw}(\lambda)$, and backscatter due to particles, $b_{bp}(\lambda)$. Some terms are constants, such as $F_0(\lambda)$, n_w, $a_w(\lambda)$, $b_{bw}(\lambda)$, or are assumed constant, such as t and g_i. The remaining IOP terms are modeled as:

$$a_{ph}(\lambda) = \text{chl } a\, a^*_{ph}(\lambda) \quad (2)$$

$$a_{cdm}(\lambda) = a_{cdm}(\lambda_0)\exp(-S_{cdm}(\lambda - \lambda_0)) \quad (3)$$

$$b_{bp}(\lambda) = b_{bp}(\lambda_0)(\lambda/\lambda_0)^{-\eta} \quad (4)$$

where η is the power law exponent describing spectral variability of b_{bp}, and λ_0 is the wavelength of normalization, which in this case was 443 nm. Each component is expressed in terms of a spectral shape parameter (i.e., $a^*_{ph}(\lambda)$, S_{cdm}, and η) which is defined in the model, and a magnitude (chl a, $a_{cdm}(443)$, $b_{bp}(443)$) that is unknown and returned by the model.

The parameterization of GSM01-CB was based on bio-optical observations obtained in CB/MAB during 1996–2002. The magnitude and variability of measured IOPs and AOPs was quantified for the CB/MAB and compared to SeaBAM data used to develop GSM01. Model parameters $a^*_{ph}(\lambda)$ and S_{cdm} were derived from field measurements and selected to reflect regional and seasonal variability. No direct measurements of scattering in CB/MAB were made on these cruises. Therefore, the parameter η in GSM01-CB was estimated based on literature values. Interannual variability and finer scale regional variability observed for $a^*_{ph}(\lambda)$ and S_{cdm} are presented, as are suggestions for refinement of the model.

2.2. Data preparation

Seasonal cruises (April, July/August, October) were conducted in CB from 1996 through 2002. Approximately 10–15 stations were occupied on each cruise. Additional cruises in MAB were conducted in August 1996, May 1997, August 1997, July 1998, and September 1998. Details of sampling and analyses provided in Harding et al. (submitted for publication) are briefly summarized here.

Water samples were collected using a rosette sampler equipped with an array of Niskin bottles. Particulate material from surface water was collected on 25 mm diameter Whatman GF/F glass fiber filters. Particulate absorption was determined on a Shimadzu UV-2401PC UV–VIS dual-beam spectrophotometer (300–800 nm). Hot methanol extraction (Kishino et al., 1985) was used to distinguish pigmented, a_{ph}, and non-pigmented, a_d, components. A scattering correction was applied by subtracting the average absorbance for 720–780 nm. Absorption coefficients were determined according to Mitchell (1990). We derived an empirical pathlength amplification factor, β, using algal cultures of CB isolates, and used this β value in all calculations of particulate absorption coefficients. Phytoplankton absorption spectra, $a_{ph}(\lambda)$, were normalized to chl a to give chl a-specific absorption spectra, $a^*_{ph}(\lambda)$. $a^*_{ph}(\lambda)$ spectra were normalized to the mean absorption for 400–700 nm, $\langle a^*_{ph}\rangle$, to obtain concentration-normalized absorption spectra, $a^*_{ph}/\langle a^*_{ph}\rangle(\lambda)$, used to distinguish variability of $a^*_{ph}(\lambda)$ associated with pigment 'packaging' (i.e., Duysens, 1956) from variability of $a^*_{ph}(\lambda)$ associated with pigment composition.

Surface water samples were filtered through 0.2 μm Nuclepore filters, and absorbance of the filtrate was measured in 10 cm cuvettes on an HP8452A Diode Array spectrophotometer (190–800 nm) against a blank of Milli-Q water. A baseline correction was made for each spectrum by subtracting the average absorbance from 720 to 780 nm. Absorption coefficients for CDOM, a_{cdom}, were calculated according to Green and Blough (1994). Spectral slope parameters, S, describing the exponential decrease of absorption with increased wavelength for CDOM, detrital material, and CDOM plus detrital material (CDM) were determined using both a linear fit to the natural log of the absorption coefficient vs. wavelength, and an exponential decay curve fit to the absorption coefficient vs. wavelength. S values were calculated for wavelength intervals starting at 300 and 400 nm and extending through the visible spectrum to 650 nm.

Discrete samples were collected to measure dissolved inorganic nutrients (NO_3^-, NO_2^-, NH_4^+, PO_4^{3-}, SiO_4) using a Technicon AutoAnalyzer II, and chl a and phaeopigments using a Turner Designs model 10 fluorometer. Samples for high performance liquid chromatography (HPLC) analyses of phytoplankton pigments were collected from surface water filtered onto GF/F filters and flash frozen on dry ice. Filters were stored in a cooler containing dry ice inside a −20 °C freezer during the cruise, and then transferred to a −80 °C freezer upon return to the lab. HPLC pigment analyses were performed by Horn Point Laboratory analytical services according to methods of Van Heukelem and co-workers (Van Heukelem et al., 1994; Van Heukelem and Thomas, 2001). The software program CHEMTAX (Mackey et al., 1996) was used to reconstruct floral composition from matrices of marker carotenoid and chl a concentrations (Adolf et al., in preparation).

Data for freshwater flow from the Susquehanna River were obtained from the U.S. Geological Survey (USGS) for the gauging station at the Conowingo Dam.

Additional measurements of chl *a* and phytoplankton cell counts were obtained from monitoring cruises of the EPA Chesapeake Bay Program (CBP).

Vertical profiles of spectral downwelling irradiance, E_d, and upwelling radiance, L_u, at 13 wavebands (412, 443, 455, 490, 510, 532, 550, 560, 589, 625, 671, 683, 700 nm) were obtained using a Biospherical Instruments (San Diego, CA) MER-2040 following SeaWiFS/SIMBIOS protocols (Fargion and Mueller, 2000). A deck cell radiometer (MER-2041) simultaneously measured downwelling surface irradiance, E_s, at the same wavebands. All profile data were normalized to deck measurements to account for cloud variability. Attenuation coefficients for downwelling irradiance, K_d, were assumed constant for the shallow surface mixing layers (<10 m) that occur in CB, and were determined by simple, linear regression of the natural log of E_d or L_u vs. depth (Smith and Baker, 1984, 1986). Surface values of E_d (E_d0^-) and L_u (L_u0^-) were obtained by extrapolation to the surface. E_d0^- values were transmitted through the air–sea interface assuming a constant transmission factor as:

$$E_d\,0^+ = \frac{E_d\,0^-}{0.98} \tag{5}$$

Instrument self-shading corrections were applied to all L_u0^- measurements (Gordon and Ding, 1992; Fargion and Mueller, 2000). L_u0^- values were transmitted through the air–sea interface to give L_W (Austin, 1974) as:

$$L_w = 0.54 L_u\,0^- \tag{6}$$

R_{RS} values were calculated as:

$$R_{RS} = \frac{L_W}{E_S} \tag{7}$$

While direct measurements of scattering were not available, estimates of $b_{bp}(443)$ were calculated by two methods. Estimates of $b(443)$ were calculated from measurements of K_d and a using models by Kirk (1981, 1984, 1994) derived from Monte Carlo modeling. In CB, $b(443)$ was estimated using the model of Kirk (1994) for turbid waters as:

$$\frac{K_d(z_m)}{a} = \left[1 + 0.245\frac{b}{a}\right]^{1/2} \tag{8}$$

where $K_d(z_m)$ is the attenuation coefficient at the midpoint of the euphotic zone. Estimates of $b_p(443)$ for MAB were calculated using similar equations derived for less turbid waters (Kirk, 1981, 1984) as:

$$\frac{K_d(z_m)}{a} = \frac{1}{\mu_0}\left[1 + G(\mu_0)\frac{b}{a}\right]^{1/2} \tag{9}$$

and

$$G(\mu_0) = 0.473\mu_0 - 0.218 \tag{10}$$

where μ_0 is the cosine of the solar zenith angle just below the air–sea interface, and $G(\mu_0)$ is a coefficient that describes the relative contribution of scattering to vertical attenuation of irradiance. Estimates of $b(443)$ were assumed to be primarily due to particles (i.e., $b(443) \approx b_p(443)$).

A second estimate of $b_p(443)$ was made from measurements of the beam attenuation coefficient (c) for a subset of stations (1997–2000 CB only). Beam attenuation is defined as:

$$c = a + b \tag{11}$$

A Sea-Bird SBE911 plus CTD package equipped with a transmissometer provided profiles of ca. at 660 nm, $c(660)$, at each bio-optical station. Estimates of $b(660)$ were calculated as:

$$b(660) = c(660) - a_{ph}(660) - a_d(660) - a_{cdom}(660) \tag{12}$$

where $a_{ph}(660)$, $a_d(660)$, and $a_{cdom}(660)$ were obtained from discrete samples. Measurements of $c(660)$ were made relative to water. Estimates of $b(660)$ were assumed to be primarily due to particles (i.e., $b(660) \approx b_p(660)$). We assumed particles in CB/MAB exhibited a wide range of sizes, thereby diminishing the spectral variability of b of the natural water sample, and $b_p(660) \approx b_p(443)$.

Estimates of $b_p(443)$ from both methods were converted to $b_{bp}(443)$ by assuming a backscattering ratio, b_{bp}/b_p, of 0.018 derived by Gould et al. (1999) from the data of Petzold (1972).

2.3. Model evaluation

In situ measurements of $R_{RS}(\lambda)$ from CB/MAB were used as inputs to GSM01, GSM01-CB, and OC4v.4, and model products were compared to coincident in situ measurements of chl *a* and $a_{cdm}(443)$, and to estimates of $b_{bp}(443)$. The evaluation data set was from CB/MAB cruises in 1996–2002. An initial suite of 372 coincident observations was reduced to 197 to avoid the use radiometric measurements that may have higher uncertainties due to long atmospheric pathlengths or extremely rapid attenuation with depth: stations with solar zenith angles >60° (110 stations) or $K_d(490) \geq 2.5\ m^{-1}$ (25 stations) were excluded. In addition, stations with large discrepancies between calculated values of $E_d\,0^+$ and E_s (90 stations) were excluded. Some stations were excluded for exceeding multiple criteria. The final data set consisted of 36 stations in the upper Bay, 47 stations in the mid-Bay, 46 stations in the lower Bay, and 68 stations in MAB.

GSM01-CB parameters were incorporated into SeaDAS 4.4 to evaluate the relative performance of OC4v.4, GSM01, and GSM01-CB using SeaWiFS radiances. We selected three High Resolution Picture

Transmission (HRPT) SeaWiFS images that were cloud-free throughout CB/MAB and for which we had contemporaneous in situ observations. SeaWiFS and in situ observations were compared on a regional basis by calculating spatial averages. This approach was used for two reasons. Firstly, the comparison of regional mean values avoided spatial and temporal aliasing typically encountered when direct comparisons of satellite pixel values and in situ observations are attempted in dynamic coastal environments such as CB/MAB. Secondly, this approach allowed us to evaluate how the frequency and distribution of low and negative L_{WN} within each image affected model outputs. While the fourth SeaWiFS reprocessing lessened the frequency of negative L_{WN}, low and occasionally negative L_{WN} from SeaWiFS remain a problem in estuarine and coastal waters due to unresolved issues in atmospheric correction (O'Reilly and Yoder, 2003).

We selected SeaWiFS scenes from 4 May, 2 July, and 21 October 2000 to represent spring, summer, and fall for a single year. SeaWiFS scenes for 4 May and 21 October coincided with our spring and fall bio-optical sampling cruises. No clear images were found during our summer 2000 cruise. The 2 July SeaWiFS scene was selected as it coincided with a monitoring cruise conducted by the CBP which provided measurements of chl *a*, but no measurements of IOPs or AOPs.

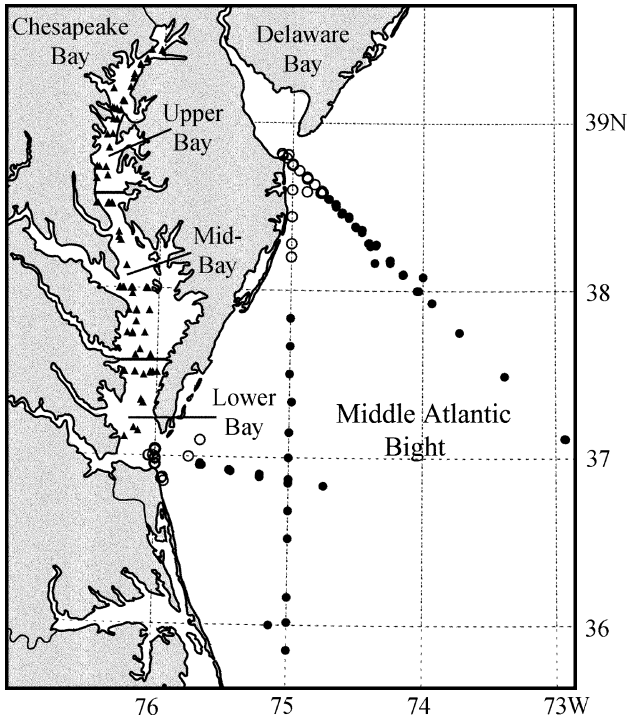

Fig. 1. CB and MAB showing stations occupied for bio-optical measurements, 1996–2002. CB is divided into three regions by latitude: upper Bay (north of 38.6°N), mid-Bay (37.6–38.6°N), and lower Bay (south of 37.6°N). Symbols indicate stations: CB (triangles), inshore MAB (open circles), and offshore MAB (filled circles).

3. Results

3.1. Regional variability of bulk optical properties

We divided CB/MAB into five regions: upper Bay (north of 38.6° N), mid-Bay (between 37.6° and 38.6° N), lower Bay (south of 37.6° N), inshore MAB, and offshore MAB (Fig. 1). a_{cdom}, a_d, and a_{ph} contributed significantly to total absorption (a) in all regions of CB/MAB (Table 1). $a(443)$, estimated as the sum of $a_{cdom}(443)$, $a_d(443)$, and $a_{ph}(443)$, ranged from $\sim 1.7\ m^{-1}$ in the upper Bay to $\sim 0.1\ m^{-1}$ in the offshore MAB. High $a_d(443)$ of $\sim 0.85\ m^{-1}$ in the turbid, upper Bay dominated $a(443)$. $a_{cdom}(443)$, $a_d(443)$, and $a_{ph}(443)$ were approximately equal contributors to $a(443)$ in the mid-Bay, lower Bay, and inshore MAB where mean $a(443)$ were $\sim 1.0, 0.8$, and $0.5\ m^{-1}$, respectively. $a(443)$ in offshore MAB was dominated by $a_{cdom}(443)$ of $\sim 0.07\ m^{-1}$, with lesser contributions from $a_{ph}(443)$ of $\sim 0.037\ m^{-1}$ and $a_d(443)$ of $\sim 0.010\ m^{-1}$. Bio-optical properties in inshore MAB resembled those of the lower Bay more than those of offshore MAB, reflecting the influences of Chesapeake and Delaware Bays on bio-optical properties of inshore waters. $a_{cdom}(443)$ was the least variable and $a_{ph}(443)$ the most variable contributor to $a(443)$ within each region.

Most CB/MAB waters had higher chl *a*, $a_{cdm}(443)$, and $b(443)$ than the SeaBAM data set used to tune GSM01 for the global ocean (Table 1). Mean chl *a*, $a_{cdm}(443)$, and $b(443)$ in CB and inshore MAB were approximately an order of magnitude higher than those used to tune GSM01. Mean chl *a* and $b(443)$ in offshore MAB were similar to values used to parameterize GSM01. However, $a_{cdm}(443)$ in offshore MAB were approximately five times higher than those used to parameterize GSM01.

Mean R_{RS} spectra for the three regions of CB were similar in shape, with maxima at green wavelengths ($\sim$560–589 nm) and minima at blue wavelengths where a_{cdom}, a_d, and a_{ph} show peaks (Fig. 2). R_{RS} spectra at green wavelengths for the mid-Bay were $\sim$25–30% lower than those for the upper and lower Bay, indicating an increase in the importance of absorption relative to scattering for the mid-Bay. Estimates of $b(555)/a(555)$ were $\sim$25–30% lower in the mid-Bay than in the upper and lower Bay (Table 1). Axial trends in the magnitudes of $R_{RS}(555)$ and $b(555)/a(555)$ were related to changes in a_{cdom}, a_{ph}, and a_d. In the upper Bay $a_d(443) \gg a_{ph}(443)$, suggesting the high $b(443)$ for the upper Bay was dominated by non-pigmented particles that typically have higher indices of refraction and scatter light more efficiently than phytoplankton. The decrease of $b(555)/a(555)$ from the upper Bay to the mid-Bay corresponded to a sharp decrease of $b(443)$, and a shift to more even

Table 1
Regional mean ± SD and range of salinity, chl *a*, $a_{cdom}(443)$, $a_d(443)$, $a_{ph}(443)$, $b(443)$, $b(555)/a(555)$, and $K_d(443)$ for the upper Bay, mid-Bay, lower Bay, inshore MAB, and offshore MAB. Field data were collected 1996–2000 at 265 stations in Chesapeake Bay, and 110 stations in the MAB. Mean values of chl *a*, $a_{cdm}(443)$, and $b(443)$ of the GSM01 tuning data set are included for comparison

Region	Salinity	Chl *a* (mg m^{-3})	$a_{cdom}(443)$ (m^{-1})	$a_d(443)$ (m^{-1})	$a_{ph}(443)$ (m^{-1})	$b(443)$ (m^{-1})	$b(555)/a(555)$ (m^{-1})	$K_d(443)$ (m^{-1})
Upper Bay	6.3 ± 5.1 (0.08–23.0)	15.9 ± 23.4 (1.0–164.5)	0.539 ± 0.073 (0.393–2.00)	0.857 ± 0.588 (0.183–2.994)	0.377 ± 0.250 (0.043–1.433)	12.1 ± 9.4 (2.4–40.3)	21.0 ± 12.2 (5–32)	2.83 ± 2.13 (1.10–9.86)
Mid-Bay	12.9 ± 3.2 (5.8 ± 19.0)	14.2 ± 10.9 (4.3–72.4)	0.368 ± 0.076 (0.209–0.505)	0.308 ± 0.151 (0.071–0.819)	0.357 ± 0.118 (0.124–0.661)	4.7 ± 5.2 (4.2–43.0)	14.5 ± 7.5 (2.8–40)	1.49 ± 0.49 (0.85–3.35)
Lower Bay	20.8 ± 4.9 (10.1–30.1)	10.3 ± 9.4 (2.2–51.0)	0.284 ± 0.090 (0.153–0.548)	0.230 ± 0.086 (0.086–0.488)	0.291 ± 0.179 (0.032–0.800)	4.6 ± 2.4 (1.0–10.3)	19.7 ± 11.9 (0.9–58)	1.19 ± 0.36 (0.59–2.36)
Inshore MAB	28.9 ± 3.2 (16.0–31.6)	4.4 ± 8.8 (0.14–44.2)	0.168 ± 0.057 (0.062–0.318)	0.162 ± 0.155 (0.006–0.494)	0.184 ± 0.158 (0.025–0.800)	2.8 ± 2.3 (0.4–9.5)	14.3 ± 9.5 (3.3–40)	0.65 ± 0.45 (0.12–1.36)
Offshore MAB	31.2 ± 0.81 (28.8–33.9)	0.36 ± 0.43 (0.06–3.2)	0.070 ± 0.035 (0.015–0.162)	0.009 ± 0.006 (0.001–0.032)	0.037 ± 0.024 (0.016–0.175)	0.75 ± 0.78 (0.3–6.8)	8.8 ± 7.0 (2.9–45)	0.13 ± 0.07 (0.05–0.87)
GSM01[a]	–	0.578 (0.023–9.93)	0.017 (0.0004–0.414)		–	0.077 (0.02–0.55)	–	–

[a] Mean values of chl *a*, the combined absorption due to CDOM and non-pigmented particulate matter, $a_{cdm}(443)$, and $b(443)$ used to tune GSM01 for the global ocean (Maritorena et al., 2002). Maritorena et al. (2002) reported a mean $b_{bp}(443)$ value for the global tuning dataset of 0.0013 m^{-1}. This value was converted to $b(443)$ using a particle backscattering ratio of 0.018 (Gould et al., 1999), and a scattering coefficient of water at 443 nm of 0.00478 m^{-1} (Smith and Baker, 1981).

particle composition. $a_d(443)$ decreased sharply and $a_{ph}(443)$ remained unchanged. Estimates of $b(443)$ in the lower Bay were the same as in the mid-Bay. Increases of $R_{RS}(555)$ and $b(555)/a(555)$ in the lower Bay were associated with 20–25% decreases of absorption by all fractions that maintained the relative contributions by pigmented and non-pigmented particles, but increased overall water clarity. The wavelength of maximum R_{RS} shifted slightly toward the blue with distance down the Bay and to inshore MAB. The mean spectral shape of R_{RS} for inshore MAB was more similar to that of CB than of offshore MAB where maximum R_{RS} was ~490 nm.

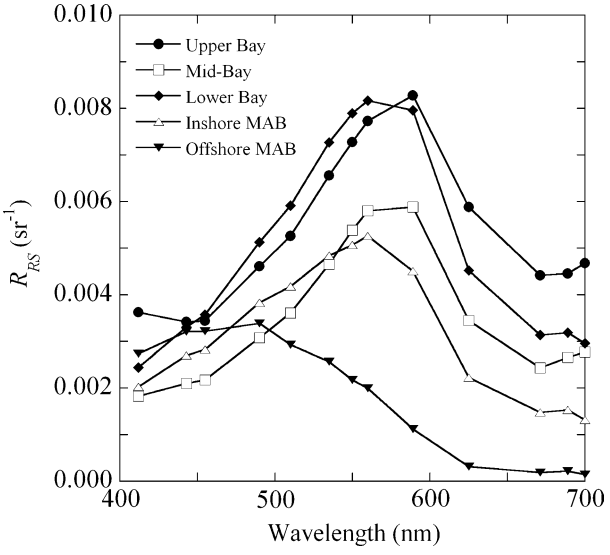

Fig. 2. Mean R_{RS} spectra for each region.

3.2. Parameterization of GSM01-CB

3.2.1. $a^*_{ph}(\lambda)$

Parameterization of GSM01-CB was based on variability of $a^*_{ph}(\lambda)$ on regional, seasonal, and interannual scales. Variability of $a^*_{ph}(\lambda)$ can result from changes in the magnitude of absorption associated with pigment concentration and cell size, i.e., the package effect, or changes in spectral shape associated with pigment composition. Normalization of $a^*_{ph}(\lambda)$ to mean absorption, as $a^*_{ph}/\langle a^*_{ph}\rangle(\lambda)$, minimizes the effect of pigment packaging while retaining variability due to pigment composition. We compared mean and standard deviation spectra for $a^*_{ph}(\lambda)$ and $a^*_{ph}/\langle a^*_{ph}\rangle(\lambda)$ to estimate the relative importance of pigment packaging and pigment composition on variability of $a^*_{ph}(\lambda)$ in CB, inshore MAB, and offshore MAB. In CB, the standard deviation spectra for $a^*_{ph}(\lambda)$ had a similar shape as the mean spectra, suggesting variations of pigment packaging dominated the variance (Fig. 3). Standard deviation spectra for $a^*_{ph}/\langle a^*_{ph}\rangle(\lambda)$ did not resemble the shape of the mean spectra, demonstrating that variability due to pigment packaging was removed. There was a significant reduction of variance for $a^*_{ph}/\langle a^*_{ph}\rangle(\lambda)$ compared to that for $a^*_{ph}(\lambda)$ (Fig. 3). The coefficient of variation (CV) at 443 nm decreased from 0.43 for $a^*_{ph}(\lambda)$ to 0.10 for $a^*_{ph}/\langle a^*_{ph}\rangle(\lambda)$, indicating ~77% reduction of variance in CB after removal of pigment packaging effects (Table 2). Similar reductions of variance for $a^*_{ph}/\langle a^*_{ph}\rangle(443)$ compared to $a^*_{ph}(443)$ occurred for data from inshore and offshore MAB. Therefore, most of the variability of $a^*_{ph}(\lambda)$ within each region could be attributed to variations of pigment packaging, with variations in pigment composition playing a secondary role (Table 2).

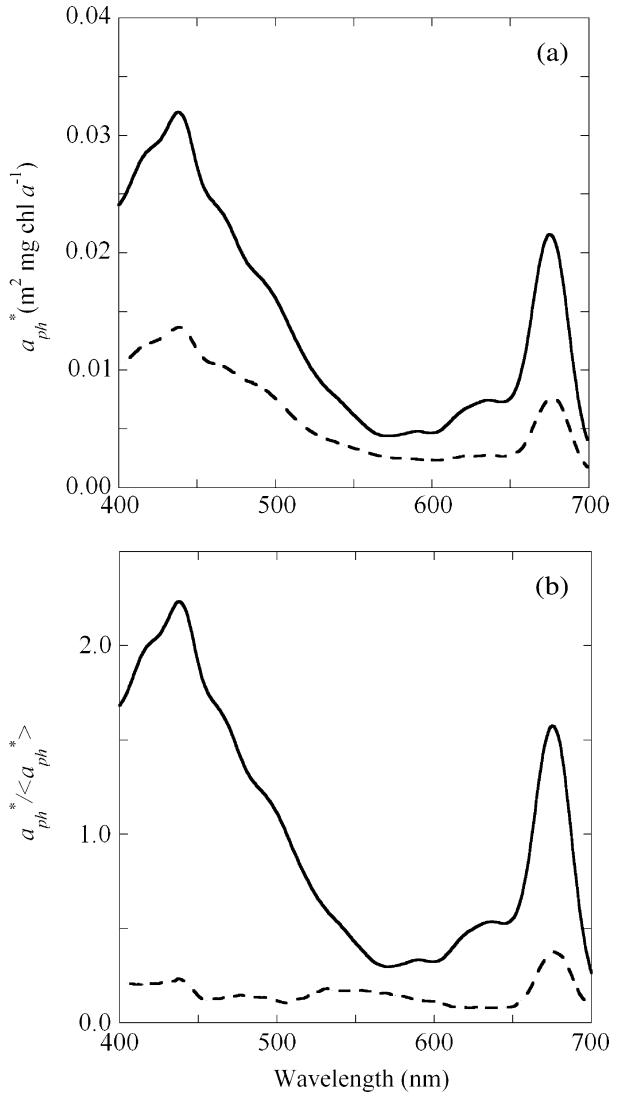

Fig. 3. Seasonal mean (solid) and standard deviation (dashed) of: (a) a^*_{ph}; (b) $a_{ph}/\langle a^*_{ph}\rangle$ spectra for CB.

The magnitude of mean $a^*_{ph}(\lambda)$ in the blue region of the spectrum exhibited a five-fold increase from CB to MAB (Fig. 4). The magnitude of $a^*_{ph}(\lambda)$ also varied seasonally in CB proper. Mean $a^*_{ph}(\lambda)$ in spring were consistently lowest and mean $a^*_{ph}(\lambda)$ in summer were consistently highest. Seasonal variability was greater in the mid- and lower Bay than in the upper Bay. Our sampling frequency was not sufficient to support a seasonal analysis in MAB.

Table 2
Coefficient of variation (SD/mean) for $a^*_{ph}(443)$ and $a^*_{ph}/\langle a^*_{ph}\rangle(443)$ for Chesapeake Bay, inshore MAB, and offshore MAB

Region	Coefficient of variation	
	$a^*_{ph}(443)$	$a^*_{ph}/\langle a^*_{ph}\rangle(443)$
All bay ($n = 216$)	0.43	0.10
Inshore MAB ($n = 26$)	0.46	0.11
Offshore MAB ($n = 75$)	0.46	0.19

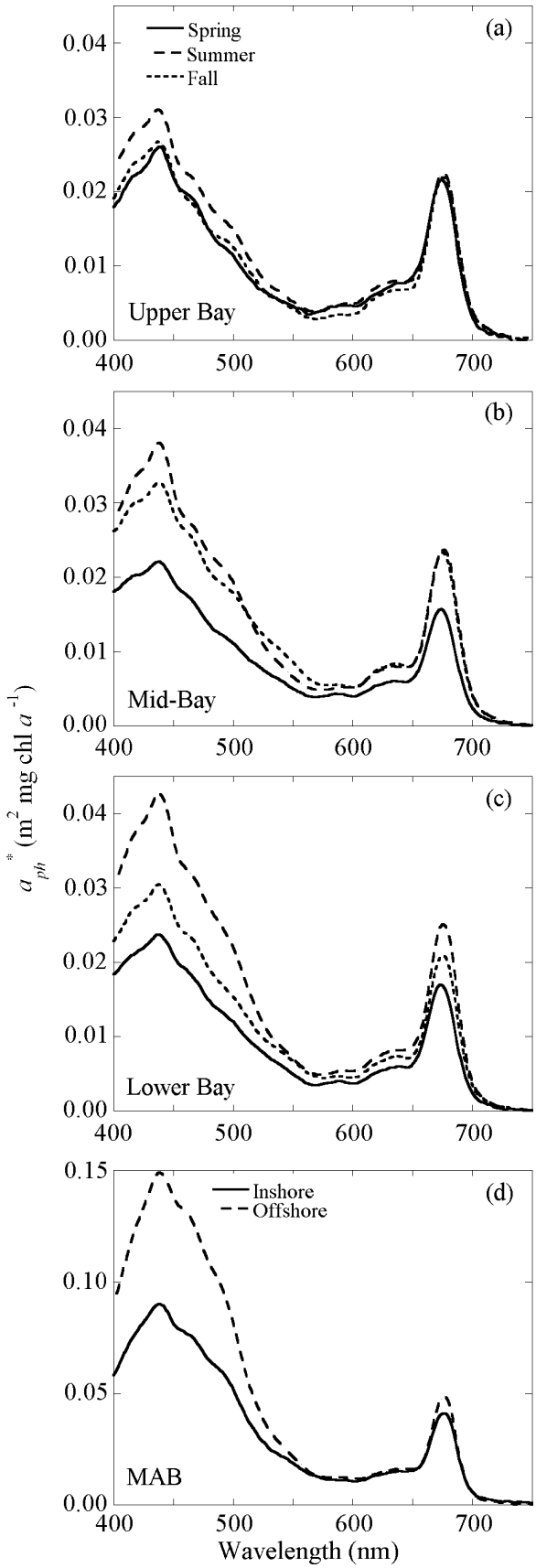

Fig. 4. Seasonal mean a^*_{ph} spectra for: (a) upper Bay; (b) mid-Bay; (c) lower Bay; (d) MAB.

We examined seasonal variability of $a^*_{ph}(\lambda)$ with respect to changes in species composition and concomitant changes in mean cell size and 'packaging' of pigments. HPLC analyses of pigment composition allowed us to quantify the fraction of total chl *a* attributed to diatoms ($f_$chl $a^{diatoms}$). We used $f_$chl $a^{diatoms}$ to investigate the relationship between seasonal transitions of floral composition and the magnitude of $a^*_{ph}(443)$. Seasonal (spring, summer, and fall) mean $f_$chl $a^{diatoms}$ for 1996–2000 was correlated ($R^2 = 0.71$) with seasonal mean $a^*_{ph}(443)$ (Fig. 5). Low mean $a^*_{ph}(443)$ in spring was associated with high $f_$chl $a^{diatoms}$, whereas high mean $a^*_{ph}(443)$ in summer was associated with low $f_$chl $a^{diatoms}$. Values of $f_$chl $a^{diatoms}$ and $a^*_{ph}(443)$ in fall were intermediate.

We inferred that seasonal changes in mean cell size suggested by $f_$chl $a^{diatoms}$ were associated with nutrient availability. The largest source of inorganic nutrients to CB is the Susquehanna River (Fisher et al., 1988, 1992). Susquehanna River flow and DIN loading were highly correlated at monthly time scales ($R^2 = 0.98$), permitting flow to serve as a proxy for nutrient loading. We investigated effects of seasonal and interannual variability of freshwater flow on $a^*_{ph}(\lambda)$. The seasonal mean $a^*_{ph}(443)$ for each cruise deviated from the five-year seasonal mean by nearly 50% (Fig. 6). Years of below-average seasonal mean $a^*_{ph}(443)$ coincided with years of above-average freshwater flow in spring and summer. Excluding fall data, we found cumulative Susquehanna River flow during the 60 days prior to sampling explained most of the variance of seasonal mean $a^*_{ph}(443)$ ($R^2 = 0.86$) (Fig. 7).

GSM01-CB was parameterized to reflect regional and seasonal variability in the field data. Analyses of

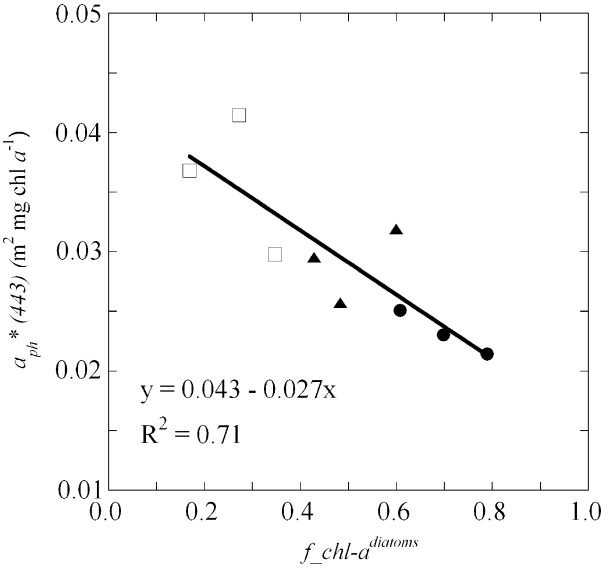

Fig. 5. Relationship between seasonal mean $f_$chl $a^{diatoms}$ and $a^*_{ph}(443)$ for 1996–2000: spring (circles), summer (squares) and fall (triangles).

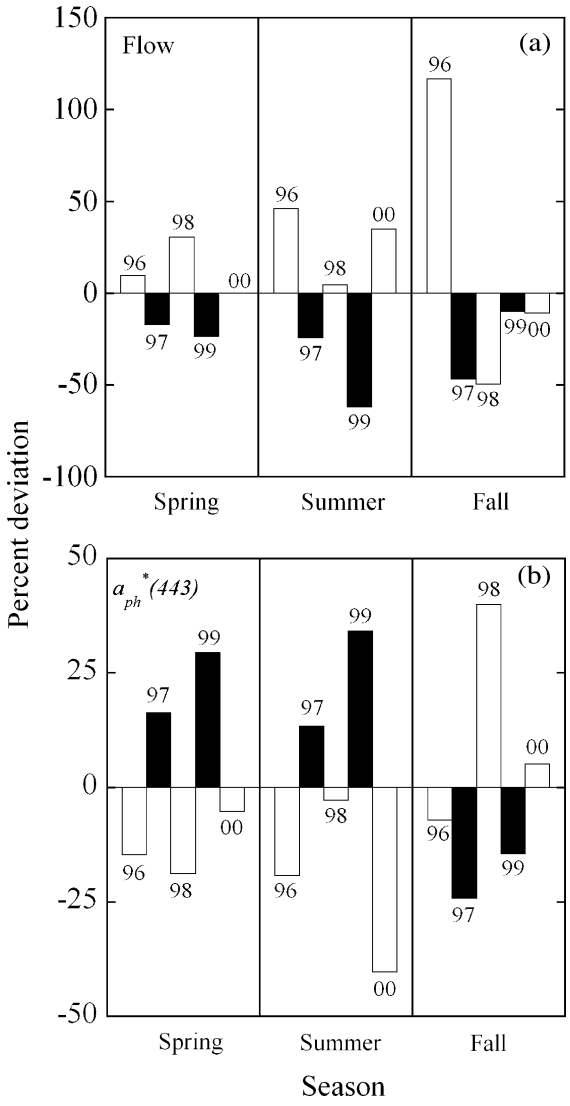

Fig. 6. (a) Freshwater flow of the Susquehanna River for the 60 days preceding each cruise, expressed as the percent deviation from the five-year seasonal mean; (b) seasonal mean $a^*_{ph}(443)$ expressed as percent deviation from the five-year seasonal mean.

variance (ANOVAs) were used to determine the statistical significance of regional and seasonal variability of $a^*_{ph}(\lambda)$. ANOVAs showed that seasonal mean $\langle a^*_{ph}\rangle$ for the mid-Bay and lower Bay were significantly different (Table 3). Within each season, mean $\langle a^*_{ph}\rangle$ for the mid- and lower Bay were not significantly different such that the mid- and lower Bay could be treated as one region (Table 4). The upper Bay was treated separately because of high turbidity and a relatively low contribution of pigmented material to the particulate load that complicated the methanol extraction procedure. Spectra with $a^*_{ph}(412) > a^*_{ph}(443)$ were excluded, often limiting the sample size for spring in the upper Bay. While field data did not indicate statistically significantly seasonal differences for $a^*_{ph}(\lambda)$ in the upper Bay, seasonal trends in the upper Bay were consistent with seasonal trends in

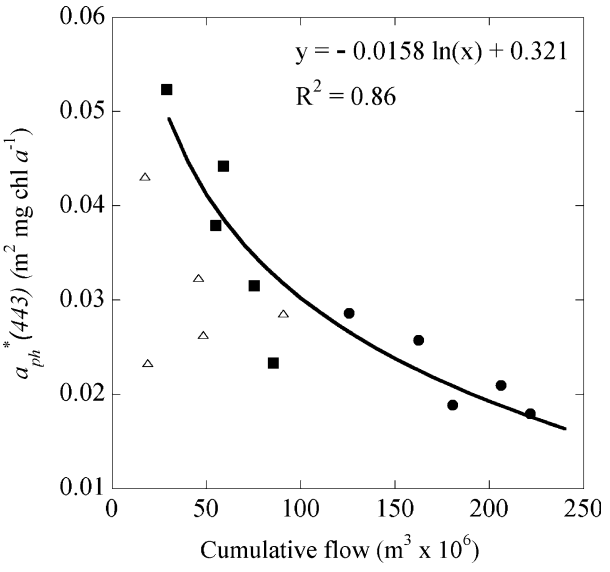

Fig. 7. Relationship between mean $a^*_{ph}(443)$ in the mid- and lower Bay for each cruise and cumulative freshwater flow from the Susquehanna River during the 60 days prior to each sampling cruise: spring cruises (circles), summer cruises (squares) and fall cruises (triangles). Curve is fit to spring and summer data only.

the mid- and lower Bay. For that reason, we chose to maintain the seasonal parameterization of $a^*_{ph}(\lambda)$ for the upper Bay as we did for the combined mid- and lower Bay region (Fig. 8; Table 5). Mean $a^*_{ph}(\lambda)$ for inshore and offshore MAB were significantly different (Table 4), supporting a regional parameterization of $a^*_{ph}(\lambda)$ for MAB (Table 5).

3.2.2. S_{cdm}

S_{cdm} increased with distance offshore, and the distribution of S_{cdm} along the salinity gradient reflected the relative contributions of a_{cdom} and a_d to a_{cdm} (Fig. 9). S_{cdom} ranged from ~0.015 to 0.020, S_d ranged from ~0.006 to 0.012, and S_{cdm} values ranged from ~0.010 to 0.018 in CB. In the uppermost Bay, S_{cdm} approached values of ~0.010, reflecting the greater contribution of a_d to a_{cdm}. In the mid- and lower Bay where a_{cdom} and a_d contributed equally to a_{cdm}, S_{cdm} ranged from 0.012 to 0.017, intermediate between S_{cdom}

Table 3
ANOVAs of seasonal differences in the magnitude of $a^*_{ph}(\lambda)$ in the Bay. ANOVAs were performed on the spectral average $a^*_{ph}(\lambda)$ between 400 and 700 nm, $\langle a^*_{ph}\rangle$

Region	n	ANOVA of seasonal differences in $\langle a^*_{ph}\rangle$		
		F	F_{crit}	P
Upper Bay	$n_{spring} = 2$; $n_{summer} = 36$; $n_{fall} = 13$	0.45	3.19	0.64
Mid-Bay	$n_{spring} = 21$; $n_{summer} = 39$; $n_{fall} = 28$	5.92	3.10	0.0039
Lower Bay	$n_{spring} = 18$; $n_{summer} = 34$; $n_{fall} = 25$	19.47	3.12	0.00000016

Table 4
ANOVAs of regional differences in the magnitude of $a^*_{ph}(\lambda)$ in the mid- and lower Bay by season, and the inshore and offshore MAB. ANOVAs were performed on the spectral average $a^*_{ph}(\lambda)$ between 400 and 700 nm, $\langle a^*_{ph}\rangle$

Region	n	ANOVA of seasonal differences in $\langle a^*_{ph}\rangle$		
		F	F_{crit}	P
Spring	$n_{mid} = 21$; $n_{low} = 18$	0.29	4.10	0.59
Summer	$n_{mid} = 39$; $n_{low} = 34$	1.57	3.97	0.21
Fall	$n_{mid} = 28$; $n_{low} = 25$	0.99	4.03	0.32
MAB	$n_{inshore} = 26$; $n_{offshore} = 75$	18.65	4.03	0.000037

and S_d. S_{cdm} in MAB was highly variable, ranging from 0.015 to 0.030. S_{cdm} was primarily influenced by CDOM in offshore MAB, as the relative contribution of a_d to a_{cdm} was always less than 40% and usually less than 20%. S_{cdm} did not show a strong relationship with salinity, but was inversely related to $a_{cdm}(443)$ (Fig. 10).

S values calculated using different fitting techniques (linear vs. non-linear) and wavelength ranges (starting at 300 nm or 400 nm) revealed similar regional trends, despite slight differences in overall magnitude (Table 6). Higher S values were obtained using the non-linear fit, consistent with previous studies (Blough and Del Vecchio, 2002). S values were higher when the 300–400 nm interval was included (Table 6), as found by Stedmon et al. (2000). S_{cdm} values used to parameterize GSM01-CB were computed using the 400–650 nm region of the spectrum and the non-linear approach. The 400–650 nm region was selected because bio-optical models used in satellite remote sensing are restricted to the visible spectrum. The non-linear fitting approach

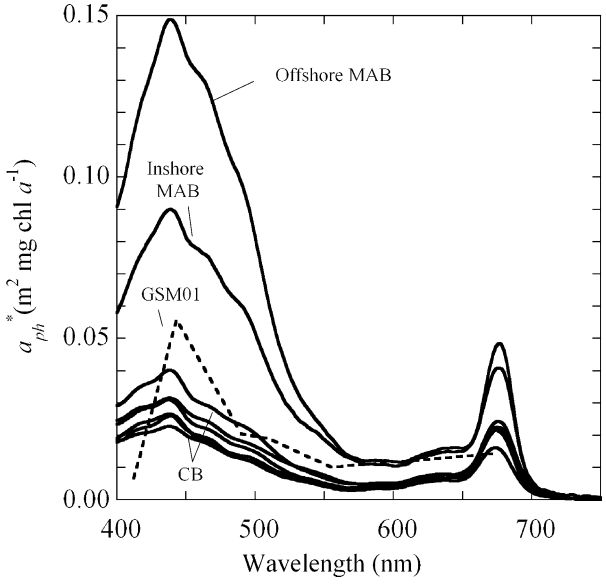

Fig. 8. Comparison of mean a^*_{ph} spectra used to parameterize GSM01-CB (solid lines), and a^*_{ph} values used in the globally optimized GSM01 (dashed line).

Table 5
Parameter values used in GSM01 and GSM01-CB

Region	Season	$a^*_{ph}(412)$	$a^*_{ph}(443)$	$a^*_{ph}(490)$	$a^*_{ph}(510)$	$a^*_{ph}(555)$	$a^*_{ph}(671)$	S_{cdm}	η
GSM01		0.00665	0.05582	0.02055	0.01910	0.01015	0.01424	0.02061	1.03373
GSM01-CB									
Upper bay	Spring	0.02119	0.02509	0.01282	0.00910	0.00427	0.02087	0.01218	0
	Summer	0.02653	0.02979	0.01655	0.01208	0.00470	0.02122	0.01218	0
	Fall	0.02259	0.02573	0.01372	0.01019	0.00376	0.02066	0.01218	0
Mid-bay	Spring	0.02001	0.02212	0.01279	0.00974	0.00449	0.01588	0.01385	0
	Summer	0.03345	0.03900	0.02318	0.01664	0.00609	0.02285	0.01385	0
	Fall	0.02758	0.03080	0.01826	0.01438	0.00691	0.02112	0.01385	0
Lower bay	Spring	0.02001	0.02212	0.01279	0.00974	0.00449	0.01588	0.01330	0
	Summer	0.03345	0.03900	0.02318	0.01664	0.00609	0.02285	0.01330	0
	Fall	0.02758	0.03080	0.01826	0.01438	0.00691	0.02112	0.01330	0
Inshore		0.07123	0.08843	0.06024	0.04072	0.01693	0.03815	0.01236	0
Offshore		0.11331	0.14678	0.09832	0.06048	0.01920	0.04349	0.01646	1

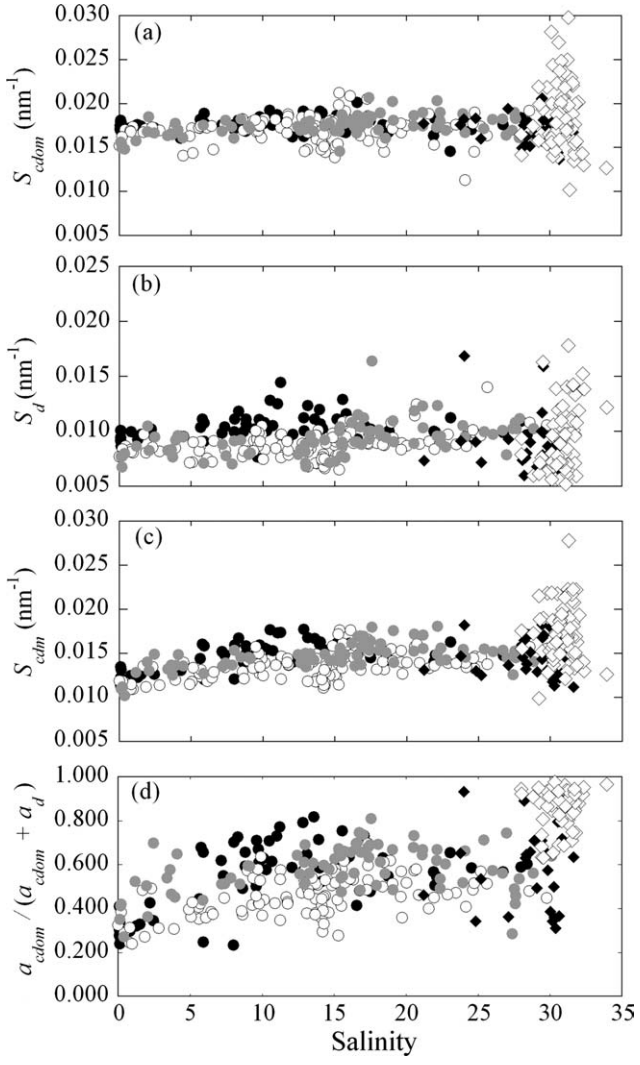

Fig. 9. (a) S_{cdom}; (b) S_d; (c) S_{cdm} values for CB and MAB calculated using the non-linear fitting technique over the wavelength interval 400–650 nm; (d) relative importance of $a_{cdom}(443)$ to the combined absorption of $a_{cdom}(443) + a_d(443)$. Circles represent seasonal values for CB stations: spring (black filled circles), summer (open circles), fall (gray circles). Diamonds represent inshore MAB stations (black filled diamonds) and offshore MAB stations (open diamonds).

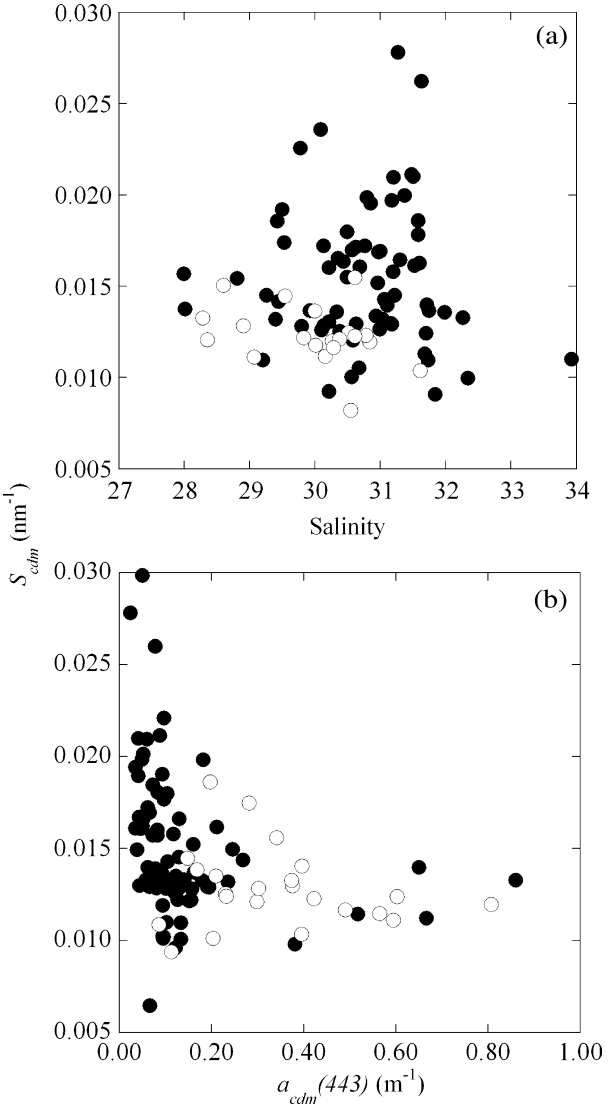

Fig. 10. S_{cdm} values for MAB plotted as function of: (a) salinity; (b) $a_{cdm}(443)$ for the inshore (open circles) and offshore (filled circles) region.

Table 6
Regional means ± SD of S_{cdm} using nonlinear and linear fitting techniques and two different wavelength intervals

Fitting technique	Upper Bay ($n = 82$)	Mid-Bay ($n = 92$)	Lower Bay ($n = 80$)	Inshore MAB ($n = 30$)	Offshore MAB ($n = 75$)
Nonlinear fit					
300–650 nm	0.01290 ± 0.00134	0.01490 ± 0.00138	0.01485 ± 0.00107	0.01397 ± 0.00180	0.01748 ± 0.00400
400–650 nm	0.01218 ± 0.00107	0.01385 ± 0.00139	0.01330 ± 0.00180	0.01236 ± 0.00164	0.01646 ± 0.00646
Linear fit					
300–650 nm	0.01230 ± 0.00105	0.01397 ± 0.00144	0.01349 ± 0.00119	0.01352 ± 0.00190	0.01762 ± 0.00315
400–650 nm	0.01204 ± 0.00108	0.01328 ± 0.00173	0.01239 ± 0.00143	0.01240 ± 0.00167	0.01515 ± 0.00384

applies a more appropriate weighting of the absorption spectrum, compared to the linear fit of log transformed data that relies more heavily on the low absorption/high wavelength region of the spectrum (Blough and Del Vecchio, 2002). ANOVAs revealed significant regional differences of annual mean S_{cdm} for the upper, mid-, and lower CB, but no significant seasonal differences of S_{cdm} (Table 7).

3.2.3. η

Scattering coefficients in natural waters reflect the combined contributions of phytoplankton, detrital, and mineral particles. Measurements of scattering by phytoplankton indicate η varies from 0 to −4 (Bricaud et al., 1983; Stramski and Kiefer, 1991). In CB $a_d(443) \geq a_{ph}(443)$, indicating particle scattering was dominated by detrital and inorganic particles rather than phytoplankton. Particles in CB/MAB likely exhibit a broad size range and variable composition such that any strong wavelength dependence associated with the properties of any one particle would be diminished. Few measurements of b have been reported for turbid waters. Gould et al. (1999) found that spectral variability of b was intermediate between η values of 0 and −1 in lower CB, with small decreases of spectral slope corresponding to decreases in the magnitude of b. For the purposes of this study, we assumed minimal wavelength dependence ($\eta = 0$) in the turbid waters of CB and inshore MAB where absorption measurements indicated particle scattering was heavily influenced by non-pigmented particles, and a small wavelength dependence ($\eta = 1$) for offshore MAB where absorption measurements indicated particle scattering was dominated by phytoplankton (Table 5).

Table 7
ANOVAs of seasonal differences in S_{cdm} for each region of the Bay and regional differences in S_{cdm} throughout CB/MAB

Region	n	ANOVA of seasonal differences in S_{cdm}		
		F	F_{crit}	P
Upper Bay	$n_{spring} = 21$; $n_{summer} = 31$; $n_{fall} = 27$	0.78	3.11	0.46
Mid-Bay	$n_{spring} = 26$; $n_{summer} = 38$; $n_{fall} = 28$	0.08	3.99	0.92
Lower Bay	$n_{spring} = 15$; $n_{summer} = 34$; $n_{fall} = 33$	1.13	3.11	0.33
All regions	$n_{upper} = 82$; $n_{mid} = 92$; $n_{lower} = 79$; $n_{inshore} = 30$; $n_{offshore} = 75$	19.70	2.40	10^{-14}

3.3. Model results

Model performance over the entire range of chl a found in CB/MAB was evaluated by applying a simple, linear regression of modeled chl a on observed chl a. Chl a from the SA models showed improvement over OC4v.4 as demonstrated by slopes of 1.0049 and 1.0580 for GSM01 and GSM01-CB, respectively, and 0.698 for OC4v.4 (Fig. 11). GSM01 exhibited a small, positive bias, while GSM01-CB exhibited a larger, negative bias that was greatest in MAB.

Regional model performance was examined by comparing mean ratios of modeled and observed chl a for CB and inshore and offshore MAB (Table 8). GSM01-CB performed slightly better than OC4v.4 in CB, whereas both SA models improved upon OC4v.4 in MAB where 2- to 3-fold overestimates of chl a by OC4v.4 were reduced to <84% for GSM01 and <50% for GSM01-CB. GSM01-CB was most effective in CB and inshore MAB. GSM01 performed slightly better than GSM01-CB in offshore MAB.

$a_{cdm}(443)$ from GSM01 and GSM01-CB showed strong agreement with observed values. Simple, linear regression of $a_{cdm}(443)$ from GSM01-CB on observed $a_{cdm}(443)$ exhibited a slope of 0.971, closer to unity than the analogous slope for GSM01 of 1.154 (Fig. 11). Ratios of modeled to measured $a_{cdm}(443)$ indicated mean errors <25% for both SA models in all regions (Table 8). GSM01-CB improved the prediction of $a_{cdm}(443)$ in CB and offshore MAB where ratios indicated mean errors of ~8% and 5%, respectively, while GSM01 performed best in inshore MAB where ratios indicated mean errors for $a_{cdm}(443)$ ~1%. Results for $b_{bp}(443)$ were stronger overall for GSM01 (Fig. 11; Table 8).

Model failure was more common for GSM01-CB than GSM01. Modeled chl a outside the range 0–150 mg m^{-3}, $a_{cdm}(443)$ outside 0–10 m^{-1}, $b_{bp}(443)$ outside 0–1 m^{-1} were excluded from comparisons of model outputs presented in Fig. 11 and Table 8. GSM01

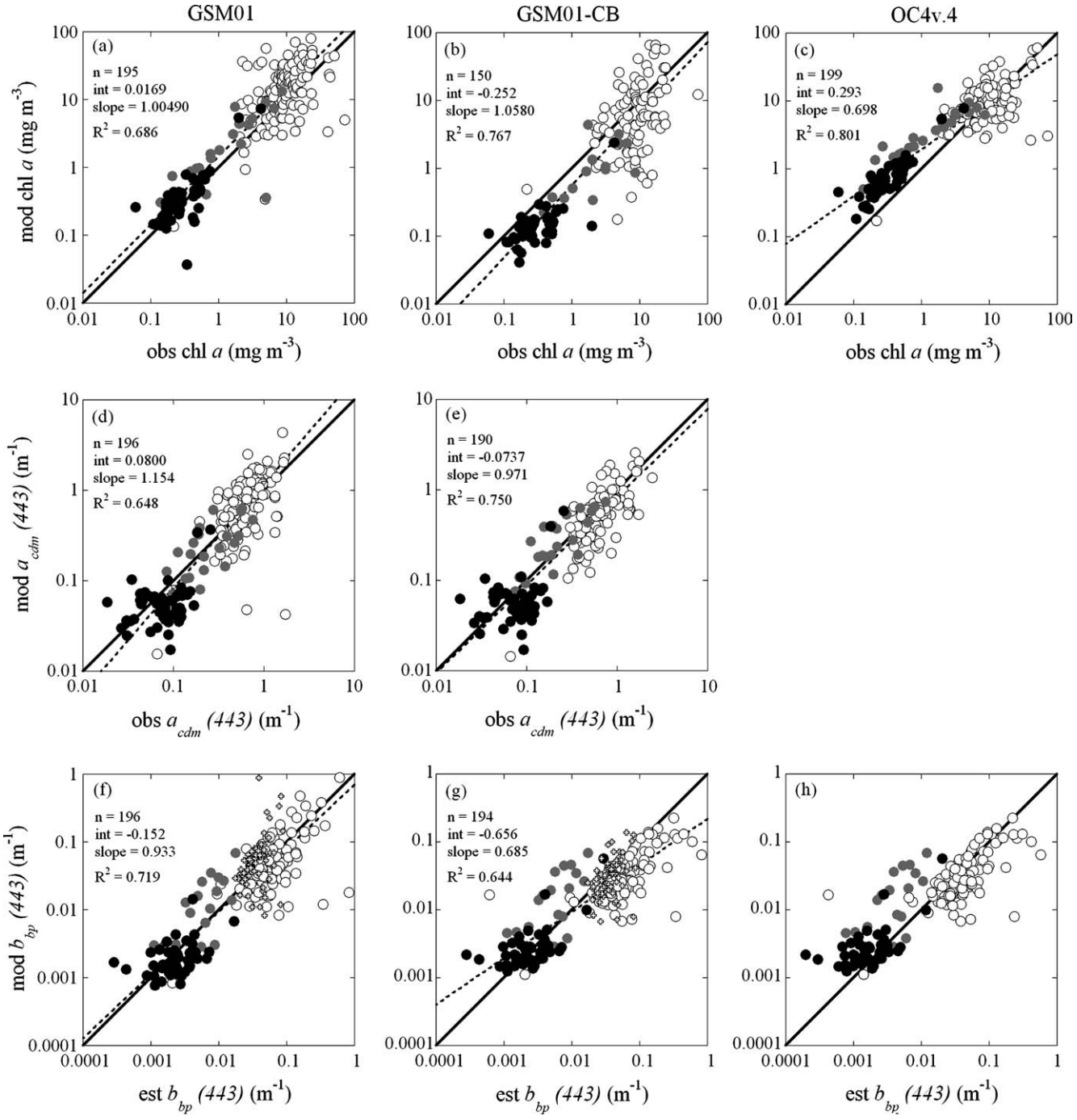

Fig. 11. Results of the GSM01, GSM01-CB, and OC4v.4 models for: (a–c) chl *a*; (d–e) $a_{cdm}(443)$; (f–g) $b_{bp}(443)$. Symbols refer to data from CB (open circles), inshore MAB (gray filled circles), and offshore MAB (black filled circles). Numbers of valid estimates returned by the model are shown as sample sizes, *n*. Estimates of $b_{bp}(443)$ calculated from irradiance and absorption measurements are shown as circles on (f–g); estimates of $b_{bp}(443)$ calculated from beam attenuation measurements are shown as plus signs on (f–g); (h) estimates of $b_{bp}(443)$ calculated from irradiance and absorption measurements using a b_b/b ratio of 0.0125 instead of 0.018.

consistently returned reasonable chl *a* for most of the 197 stations (Fig. 11). However, GSM01-CB returned 47 unreasonable estimates of chl *a*. High rates of model failure did not affect $a_{cdm}(443)$ and $b_{bp}(443)$ products from either model.

3.4. SeaWiFS applications

SeaWiFS products from OC4v.4, GSM01, and GSM01-CB were compared for CB, inshore MAB, and offshore MAB (Figs. 12, 13). SeaDAS returned OC4v.4,

Table 8
Comparison of the mean ratio (±SD) of modeled and measured chl *a* and $a_{cdm}(443)$, and estimated $b_{bp}(443)$ for Chesapeake Bay, inshore MAB, and offshore MAB

	Chesapeake Bay chl *a*	Inshore MAB chl *a*	Offshore MAB chl *a*	Chesapeake Bay $a_{cdm}(443)$	Inshore MAB $a_{cdm}(443)$	Offshore MAB $a_{cdm}(443)$	Chesapeake Bay $b_{bp}(443)$	Inshore MAB $b_{bp}(443)$	Offshore MAB $b_{bp}(443)$
GSM01	1.99 ± 2.21	1.84 ± 0.92	1.31 ± 0.68	1.24 ± 0.58	1.01 ± 0.54	0.87 ± 0.61	0.94 ± 0.65	2.28 ± 1.35	1.43 ± 0.88
GSM01-CB	1.10 ± 1.08	0.59 ± 0.57	0.51 ± 0.29	0.92 ± 0.40	1.12 ± 0.42	0.95 ± 0.67	1.35 ± 0.91	2.88 ± 1.64	1.34 ± 1.26
OC4v.4	1.20 ± 0.71	3.12 ± 2.05	2.40 ± 1.03	–	–	–	–	–	–

Mean ratio = modeled/measured.

GSM01, and GSM01-CB products for each pixel, regardless of whether any of the $L_{WN}(\lambda)$ were negative. $L_{WN}(412)$ images were included in Fig. 12 to illustrate the frequency and distribution of low $L_{WN}(412)$. Pixels with obvious problems in atmospheric correction (i.e., negative $L_{WN}(\lambda)$) were excluded (Fig. 14; Tables 9, 10). SeaWiFS products that were still outside of reasonable ranges (i.e., negative or extremely high) due to model failure were also excluded from the regional statistics.

The three HRPT images we selected covered a range of $L_{WN}(412)$ and chl *a*. The 4 May image represented a day when $L_{WN}(412)$ was negative for much of the mid- and upper Bay, but very high in inshore MAB, north and south of the CB mouth (Fig. 12a). The 2 July image represented a day with relatively high $L_{WN}(412)$ throughout the region (Fig. 12e). Finally, the 21 October image had relatively low $L_{WN}(412)$ in CB and most of MAB (Fig. 12i). GSM01 returned negative chl *a* values for pixels with negative or low $L_{WN}(412)$, as can be seen for CB in the 4 May image (Fig. 12c), and for MAB in the 21 October image (Fig. 12k). In contrast, GSM01-CB returned unreasonably high chl *a* values (i.e., often well over 100 mg m^{-3}) for pixels with negative or low $L_{WN}(412)$ in CB, as demonstrated in the 4 May image (Fig. 12d), but negative chl *a* values for pixels with negative or low $L_{WN}(412)$ in MAB, as seen in the 21 October image (Fig. 12l). GSM01 and GSM01-CB returned up to 25% fewer valid estimates of chl *a* than did OC4v.4 (Tables 9, 10). In CB, we found valid chl *a* retrievals from GSM01-CB were closest to in situ chl *a* for 4 May and 21 October data, whereas chl *a* from GSM01 were closest to in situ values for 2 July data (Table 9). In MAB, chl *a* from GSM01 and GSM01-CB were lower than chl *a* from OC4v.4, and GSM01-CB always returned lower chl *a* than GSM01 (Table 10).

In CB, SeaWiFS estimates of $a_{cdm}(443)$ from GSM01 and GSM01-CB were similar and within ~25% of in situ values (Table 9). Both SA models returned higher $a_{cdm}(443)$ in spring than fall, consistent with in situ $a_{cdm}(443)$. Estimates of $a_{cdm}(443)$ in inshore MAB were lower than in situ values (Table 10). In offshore MAB, SeaWiFS estimates of $a_{cdm}(443)$ also were similar, and within a factor of two or less of in situ values. Model failures were not a problem for $a_{cdm}(443)$ in any region of CB/MAB (Tables 9, 10).

4. Discussion

4.1. Model performance

Bio-optical complexity of Case 2 waters poses a challenge to obtain accurate estimates of chl *a* using remote sensing of ocean color. Empirical radiance ratio algorithms, such as OC4v.4 used with SeaWiFS, provide reasonable estimates of chl *a* in waters where phytoplankton dominate absorption (O'Reilly et al., 1998). SA models, such as GSM01, account for multiple constituents that absorb and scatter light, but require knowledge of the bio-optical properties of the water body of interest. The goal of research described here was to improve satellite-derived estimates of chl *a* in CB/MAB that heretofore have relied on empirical algorithms such as OC4v.4. Bio-optical properties of CB/MAB differed significantly from those of the open ocean used in the original GSM01 (Table 1), leading us to hypothesize we could improve retrievals of chl *a* for these Case 2 waters with a locally tuned SA model. SA models also provide estimates of $a_{cdm}(443)$ and $b_{bp}(443)$ not obtained from OC4v.4. We used measured values of the input parameters, $a^*_{ph}(\lambda)$ and S_{cdm} to develop GSM01-CB, a modified version of the globally parameterized GSM01.

SA models showed the most improvement over OC4.v4 in MAB. OC4v.4 attributed absorption by CDOM to absorption by phytoplankton in MAB where $a_{cdm} > a_{ph}$, resulting in a 2- to 3-fold bias for chl *a* (Table 8), and a low slope (0.698) of the regression of modeled and observed chl *a* throughout CB/MAB (Fig. 11). GSM01 and GSM01-CB separated absorption by phytoplankton from absorption by CDOM and returned chl *a* estimates within ~30% and ~50% of in situ values in CB and MAB, respectively (Table 8), greatly improving the slope of the regression of modeled on observed chl *a* across CB/MAB (Fig. 11).

The accuracy of chl *a* returned by SA models varied by region. In CB, values of $a^*_{ph}(\lambda)$ and S_{cdm} used in GSM01-CB were well constrained seasonally and regionally. The benefit of the locally tuned parameters was evident in the strong performance of GSM01-CB in CB where mean chl *a* was within 10% of in situ values. In contrast, the globally tuned GSM01 returned mean

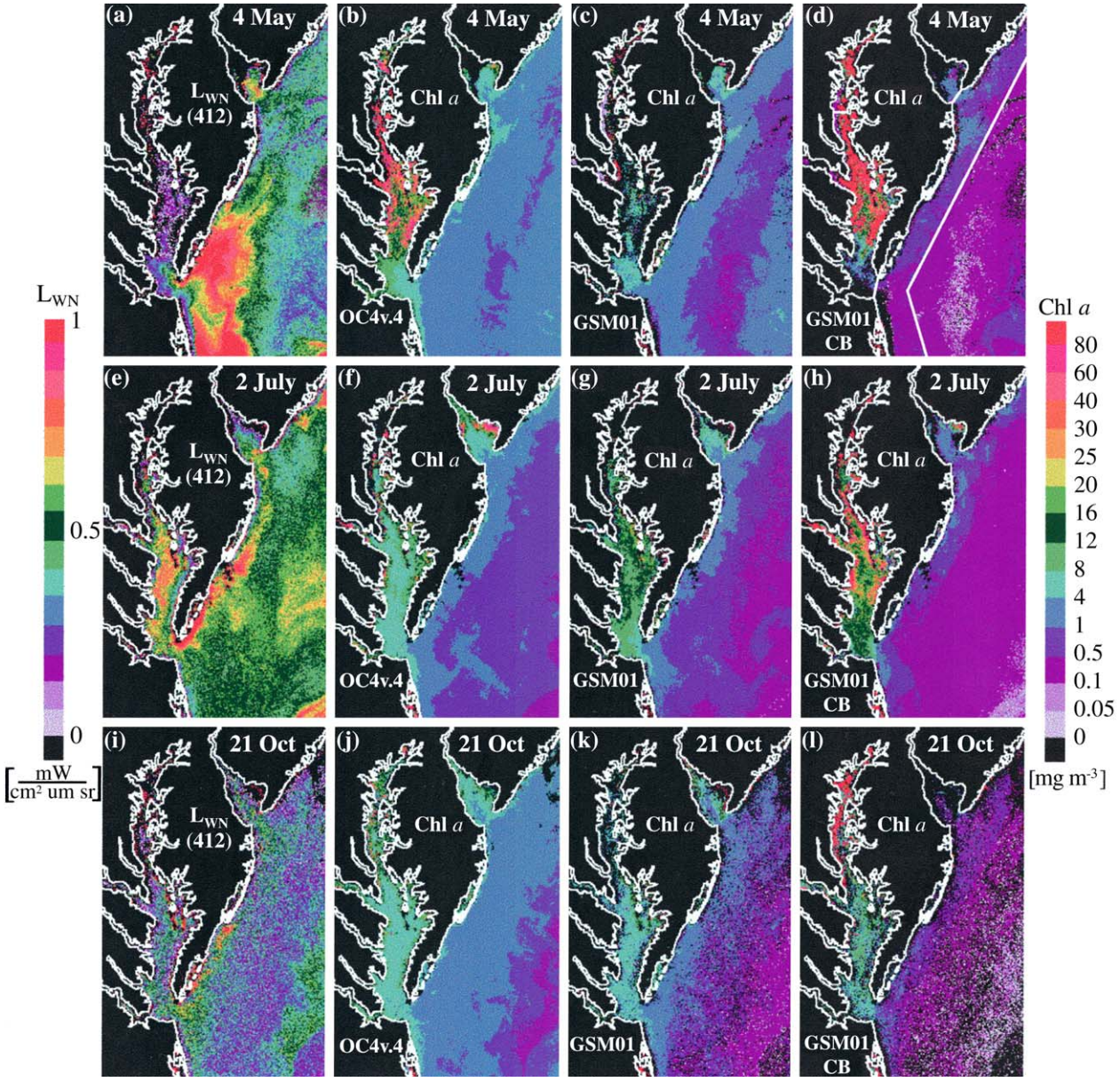

Fig. 12. SeaWiFS images of $L_{WN}(412)$ and chl *a* products from OC4v.4, GSM01 and GSM01-CB for three days in 2000: (a–d) 4 May; (e–h) 2 July; and (i–l) 21 October. White line in panel (d) indicates boundaries between CB and inshore and offshore MAB used in the calculation of regional statistics presented in Tables 9 and 10.

chl *a* that were a factor of two greater than in situ values (Table 8). In MAB, where $a^*_{ph}(\lambda)$ and S_{cdm} were less well constrained, GSM01-CB underestimated and GSM01 overestimated chl *a* by ~30–80%.

Low estimates of chl *a* in MAB by GSM01-CB could result from $a^*_{ph}(\lambda)$ parameter values that were too high. We compared values of $a^*_{ph}(675)$ from field samples to literature values of specific absorption coefficients for chl *a* in solution. Absorption coefficients for field samples with pigments contained in cells (i.e., 'packaged') should be lower than those for pigments in solution (i.e., 'unpackaged'). We found mean $a^*_{ph}(675)$ for inshore and offshore MAB were ~0.040 and 0.048 m^2 (mg chl *a*)$^{-1}$, respectively, exceeding a theoretical value for chl *a* in solution of 0.0207 m^2 (mg chl *a*)$^{-1}$ (Bricaud et al., 1983). One cause of these overestimates of $a^*_{ph}(\lambda)$ could be our correction for the pathlength amplification factor, β. We used an empirically derived β based on measurements of phytoplankton cultures isolated from CB that may not have been representative of the scattering properties of phytoplankton species throughout MAB. We compared our β to a variety of literature values of β summarized by Mitchell et al. (2002). Following the presentation of Mitchell et al. (2002), we calculated the optical density of cells in suspension (OD_{sp}) for an optical density for filtered cells

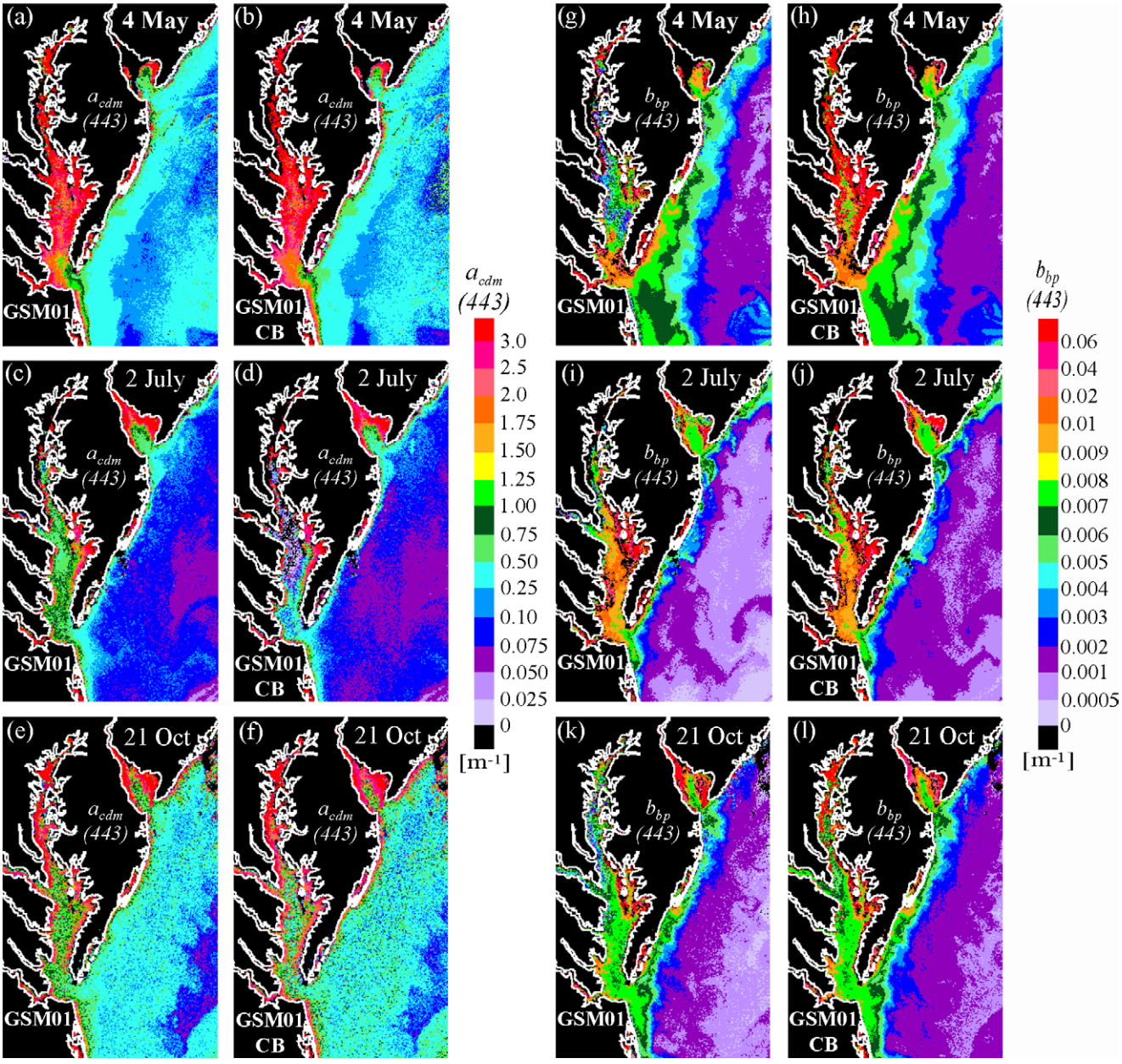

Fig. 13. SeaWiFS images of: (a–f) $a_{cdm}(443)$; (g–l) $b_{bp}(443)$ from OC4v.4, GSM01 and GSM01-CB for 4 May 2000.

(OD_{fp}) of 0.2 m^{-1} (i.e., $OD_{sp} = OD_{fp} \times \beta$) using our β. We obtained an OD_{sp} of 0.118 m^{-1}, a high value compared to the range of 0.055–0.105 m^{-1} using the 13 published β presented by Mitchell et al. (2002). This comparison demonstrated that $a^*_{ph}(\lambda)$ can vary by a factor of two depending on the choice of β, and that our β returned values at the high end of that range. The presence of phaeopigments also could explain high values of $a^*_{ph}(\lambda)$ observed in CB/MAB. Phaeopigments accounted for ~10–40% of the combined concentration of chl *a* plus phaeopigments (= pigment) in mid- and lower CB and MAB, with higher percentages in upper CB. We found normalization of $a_{ph}(\lambda)$ to pigment reduced the magnitude of seasonal and regional mean $a^*_{ph}(\lambda)$ throughout CB/MAB by ~15–30% compared to normalization to chl *a* only. High values of $a^*_{ph}(\lambda)$ due either to an inappropriate β or high concentrations of phaeopigments would cause underestimates of chl *a* values by GSM01-CB.

$a_{cdm}(443)$ from GSM01-CB was similar in magnitude to $a_{cdm}(443)$ from GSM01, suggesting $a_{cdm}(443)$ was less sensitive to the changes in parameterization than was chl *a*. Estimates of $a_{cdm}(443)$ from both SA models exhibited stronger agreement with in situ values than was found for chl *a* (Table 8). Chl *a* is more difficult to predict than $a_{cdm}(443)$ because it exhibits significantly greater variability in CB/MAB (Table 1). In addition, chl *a* is derived from a complicated relationship with

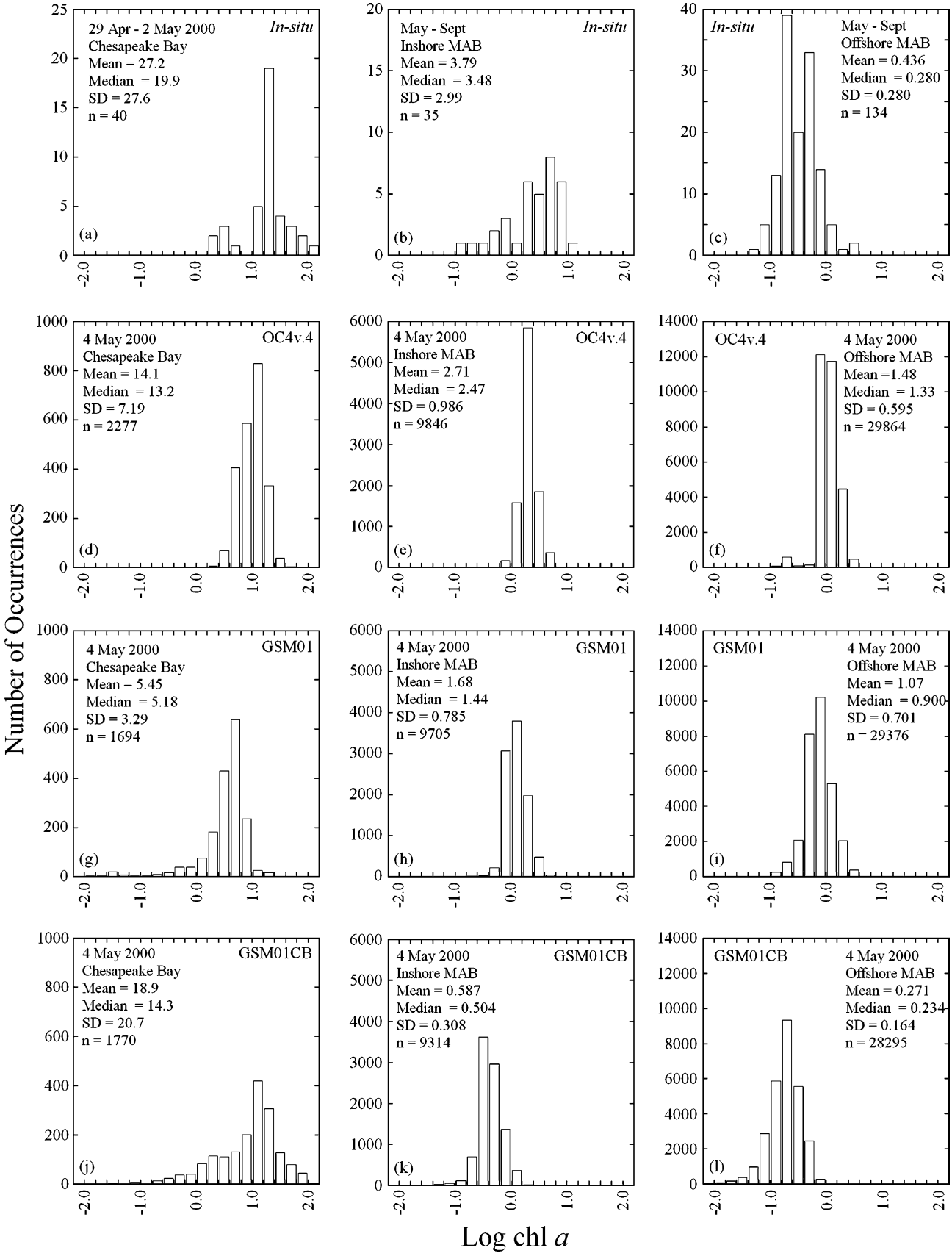

Fig. 14. Histograms of in situ and SeaWiFS chl *a* observations for CB and inshore and offshore MAB for 4 May only: (a–c) in situ; (d–f) SeaWiFS OC4v.4; (g–i) SeaWiFS GSM01; (j–l) SeaWiFS GSM01-CB.

Table 9
Comparison of in situ and SeaWiFS observations of chl *a* and $a_{cdm}(443)$ for the Chesapeake Bay region south of 38.7°N. SeaWiFS statistics were limited to pixels for which all L_{WN} were positive, and chl *a* and $a_{cdm}(443)$ were in the range of 0–150 mg m^{-3} and 0–10 m^{-1}, respectively

SeaWiFS	SeaWiFS chl *a*				SeaWiFS $a_{cdm}(443)$		
Image day	In situ[a]	OC4v.4	GSM01	GSM01-CB	In situ[a]	GSM01	GSM01-CB
4 May 2000							
Mean	27.2	14.1	5.45	18.6	0.98	0.88	1.01
Median	19.9	13.2	5.18	14.3	0.81	0.76	0.86
SD	27.6	7.19	3.29	20.7	0.68	0.43	0.67
n	40	2277	1694	1770	7	2277	2178
2 July 2000							
Mean	11.9	7.68	11.5	18.7	–	0.38	0.21
Median	11.8	7.08	11.4	16.7	–	0.32	0.12
SD	4.28	3.04	4.42	10.0	–	0.23	0.32
n	35	3285	3139	3240	–	3283	2729
21 October 2000							
Mean	9.12	6.02	5.60	6.87	0.60	0.44	0.43
Median	9.39	5.70	5.49	7.00	0.60	0.38	0.38
SD	3.19	1.58	2.43	3.96	0.14	0.22	0.26
n	67	3117	2917	2453	11	3117	3100

[a] In situ data collected 29 April–2 May, 10–14 July, and 12–21 October, 2000. No $a_{cdm}(443)$ data were available for July 2000.

absorption, whereas $a_{cdm}(443)$ is an optical property intrinsic to the bio-optical model.

Evaluation of the $b_{bp}(443)$ product was hindered by our lack of direct measurements of scattering. We compared estimates of $b_{bp}(443)$ from GSM01 and GSM01-CB to estimates of $b_{bp}(443)$ calculated from in situ measurements using two different methods. Calculation of $b_{bp}(443)$ from beam attenuation resulted in estimates of $b_{bp}(443)$ that differed by an average of $42 \pm 52\%$ from those based on diffuse attenuation and

Table 10
Comparison of in situ and SeaWiFS observations of chl *a* and $a_{cdm}(443)$ for the MAB. SeaWiFS statistics were limited to pixels for which all L_{WN} were positive, and chl *a* and $a_{cdm}(443)$ were in the range of 0–150 mg m^{-3} and 0–10 m^{-1}, respectively. See Fig. 12 for regions used in SeaWiFS statistics

	In situ[a] *May–Sept*	SeaWiFS 4 May 2000			SeaWiFS 2 July 2000			SeaWiFS 21 October 2000		
	1996–1998	OC4v.4	GSM01	GSM01-CB	OC4v.4	GSM01	GSM01-CB	OC4v.4	GSM01	GSM01-CB
Chl *a*										
Inshore										
Mean	3.79	2.71	1.68	0.59	1.49	1.15	0.61	2.23	1.47	0.54
Median	3.48	2.47	1.44	0.50	1.22	0.94	0.54	2.06	1.30	0.54
SD	2.99	0.99	0.78	0.31	0.87	0.75	0.28	0.84	0.88	0.30
n	35	9846	9705	9314	9814	9787	9798	9891	8968	7477
Offshore										
Mean	0.44	1.48	1.07	0.27	0.69	0.50	0.19	1.01	0.50	0.13
Median	0.28	1.33	0.90	0.23	0.70	0.49	0.19	1.04	0.42	0.10
SD	0.44	0.59	0.70	0.16	0.23	0.21	0.07	0.42	0.34	0.10
n	134	29864	29376	28295	30691	30690	30684	30539	25375	17305
$a_{cdm}(443)$										
Inshore								–		
Mean	0.31	–	0.16	0.17	–	0.08	0.09	–	0.18	0.21
Median	0.27	–	0.14	0.15	–	0.07	0.08	–	0.16	0.17
SD	0.18	–	0.08	0.10	–	0.04	0.05	–	0.08	0.12
n	26	–	9846	9846	–	9813	9814		9819	9819
Offshore								–		
Mean	0.08	–	0.11	0.10	–	0.06	0.06	–	0.12	0.15
Median	0.08	–	0.10	0.09	–	0.06	0.06	–	0.11	0.13
SD	0.04	–	0.06	0.04	–	0.01	0.01	–	0.06	0.08
n	79	–	29873	29872	–	30691	30691	–	30539	30539

[a] Statistics for all in situ data available for the inshore and offshore MAB.

absorption (Fig. 11f–g). In addition, both estimates of $b_{bp}(443)$ from in situ data required several assumptions about b_b/b and the spectral variability of b_b. For example, our estimates of $b_{bp}(443)$ were calculated using a constant b_b/b of 0.0180 (Gould et al., 1999). However, Sydor and Arnone (1997) derived a b_b/b of 0.0125 from measurements in coastal waters off Mississippi. Tzortziou (2004) found a mean value for b_b/b of 0.0130 from direct measurements of scattering in the mid-Bay (38.7–38.9°N), and reported that b_b/b ranged from ~0.006 to 0.025, suggesting considerable variability over a very small area. The use of a b_b/b of 0.0125 instead of 0.0180 resulted in a mean difference of ~30% in our estimates of $b_{bp}(443)$. When compared to modeled $b_{bp}(443)$, this change in estimated $b_{bp}(443)$ reduced the bias of GSM01-CB in CB, but increased the bias in MAB (Fig. 11h). The lack of direct measurements of the magnitude, variability, and spectral characteristics of scattering in the Bay poses a significant limitation in the evaluation of the $b_{bp}(443)$ product, and affects the parameterization of η in GSM01-CB.

4.2. SeaWiFS products

GSM01-CB parameters were incorporated into SeaDAS to evaluate practical applications of GSM01-CB and GSM01 in CB/MAB using currently available SeaWiFS radiances that are probably subject to atmospheric correction errors. Regional mean values of SeaWiFS products were compared to mean values of the most contemporaneous field data available (Fig. 14; Tables 9, 10). Although pixels with negative $L_{WN}(\lambda)$ were excluded from the SeaWiFS regional means, a higher number of valid chl *a* was returned by OC4v.4 than by GSM01 or GSM01-CB (Fig. 14, Tables 9, 10). The largest differences between the number of valid estimates returned by OC4v.4 and the SA models occurred where low and negative $L_{WN}(\lambda)$ were most prevalent: in CB in May and MAB in October (Figs. 12–14, Tables 9, 10). OC4v.4 avoids the use of low wavebands that are more likely to be affected by atmospheric correction errors. GSM01 and GSM01-CB use all visible SeaWiFS wavebands, and are thereby more sensitive to errors in magnitude and spectral shape of $L_{WN}(\lambda)$ that may exist even when no waveband is forced to a negative value. Despite errors in $L_{WN}(\lambda)$ that remain after removal of 'negative' pixels, we found that comparisons of SeaWiFS chl *a* from OC4v.4, GSM01, and GSM01-CB to in situ data were largely consistent with results obtained using in situ radiances. Specifically: (1) GSM01-CB performed as well or better than GSM01 and OC4v.4 in CB; (2) both SA models improved upon OC4v.4 in offshore MAB.

In CB, GSM01-CB best captured the high, spring chl *a* in May, and GSM01 chl *a* was closest to in situ mean chl *a* in July (Fig. 14; Table 9). All three models returned similar chl *a* for the October image when in situ chl *a* were close to the annual mean for CB (~9–10 mg m^{-3}). Considering the three images as a time series, GSM01-CB and OC4v.4 detected seasonal trends of chl *a* in CB better than GSM01.

In MAB, SeaWiFS products were compared to regional mean values calculated from all available in situ observations (May–September 1996–1998) as shipboard data were not available for 2000. This comparison was not optimal, but allowed us to determine if SeaWiFS products were reasonable. In offshore MAB, chl *a* from both SA models reduced the high bias of OC4v.4 chl *a* (Fig. 14; Table 10). GSM01 chl *a* were higher than in situ chl *a*, and GSM01-CB chl *a* were lower than in situ chl *a* (Table 10), consistent with results using in situ radiances as inputs (Table 8). In inshore MAB, all three models underestimated in situ chl *a* (Table 10), in contrast with results using in situ radiances as inputs wherein OC4v.4 greatly overestimated chl *a* (Table 8). This difference likely results from a sampling bias. In situ mean chl *a* were calculated from stations located in the CB and DB outflow regions (Fig. 1) where chl *a* is typically higher than for other regions of inshore MAB, whereas SeaWiFS mean chl *a* were calculated from pixels throughout inshore MABF (see Fig. 12d). Ignoring the in situ values, the SA models returned much lower chl *a* than did OC4v.4, and chl *a* from GSM01-CB were lower than chl *a* from GSM01 (Table 10), again consistent with results obtained using in situ bio-optical data as inputs to the models (Table 8).

SeaWiFS $a_{cdm}(443)$ from both SA models was reasonable in magnitude and captured expected seasonal trends. In CB, higher $a_{cdm}(443)$ were found in May than in July and October, consistent with in situ observations (May and October only) (Table 8). In MAB, lower $a_{cdm}(443)$ were found in July SeaWiFS data (Table 9), possibly indicating an effect of photobleaching during this well-stratified period (Vodecek et al., 1997, Nelson et al., 1998, Del Vecchio et al., 2002). In inshore MAB, both SA models returned lower $a_{cdm}(443)$ than the in situ values, again suggesting bias associated with the concentration of sampling stations in the CB and DB outflow regions where higher $a_{cdm}(443)$ occur. GSM01 and GSM01-CB returned similar values of $a_{cdm}(443)$, as was found when in situ radiances were used as inputs, again indicating the $a_{cdm}(443)$ product was not very sensitive to the changes in parameterization.

4.3. Model refinements

GSM01-CB was parameterized with values that captured statistically significant seasonal and regional variability of $a^*_{ph}(\lambda)$ and S_{cdm}. However, a closer examination of bio-optical data for CB/MAB suggested

alternatives to the parameterization of GSM01-CB that could improve model performance. We pursued relationships between model parameters and other variables that could refine the tuning on regional and seasonal scales addressed by GSM01-CB.

Parameterization of $a^*_{ph}(\lambda)$ in GSM01-CB did not take into account interannual variability of $a^*_{ph}(\lambda)$ observed during 1996–2000 (Fig. 6). We attempted to predict interannual variability of $a^*_{ph}(\lambda)$ from freshwater flow based on a hypothesis that nutrient availability regulated major floral transitions in CB. Regionally, we observed a pattern of increasing $a^*_{ph}(\lambda)$ from 'eutrophic' CB waters to 'oligotrophic' MAB waters (Fig. 4) that was consistent with previous studies relating nutrient availability to cell size and packaging of pigment, as well as pigment composition (Yentsch and Phinney, 1989; Bricaud et al., 1995; Cleveland, 1995). Briefly, the 'package effect' refers to a reduction of specific absorption by pigment molecules when they are contained in phytoplankton cells, due to shading of pigment molecules by other pigment molecules (Duysens, 1956; Kirk, 1975a,b; Morel and Bricaud, 1981). Large cells with greater pigment packaging are more abundant in turbulent systems with high inputs of nutrients and high chl *a*, whereas small cells with less pigment packaging predominate in systems with low nutrient concentrations and low chl *a* (Yentsch and Phinney, 1989). Low nutrient/low chl *a* waters often support phytoplankton cells with higher concentrations of accessory pigments, primarily 'photoprotective' pigments, that increase absorption per unit chl *a* in the blue region of the spectrum. We found the variability of $a^*_{ph}(\lambda)$ in each region of CB/MAB could be attributed primarily to variability in the magnitude of absorption due to changes in pigment packaging (Fig. 3).

Seasonal variability of $a^*_{ph}(\lambda)$ in CB was consistent with well-documented transitions of floral composition and associated changes of mean cell size. We found mean $a^*_{ph}(\lambda)$ in CB was highest in summer, lowest in spring, and intermediate in fall (Fig. 4). The spring flora in CB consists predominantly of large, centric diatoms (Malone et al., 1988; Marshall and Nesius, 1996) with relatively high pigment packaging and low $a^*_{ph}(\lambda)$. Summer marks the transition to a more diverse flora consisting of smaller, flagellated, cells (Malone et al, 1991; Malone, 1992; Marshall and Nesius, 1996) associated with less packaging of pigments relative to the spring flora, and higher $a^*_{ph}(\lambda)$. The fall flora typically consists of a less diverse community and the re-emergence of large cells, including diatoms (Marshall and Nesius, 1996), with higher pigment packaging and lower $a^*_{ph}(\lambda)$. The negative correlation of seasonal mean $f\_\text{chl}\ a^{\text{diatoms}}$ and $a^*_{ph}(443)$ in CB (Fig. 5) suggests a relationship between cell size and $a^*_{ph}(\lambda)$ that has been documented by direct measurements in other coastal waters (Ciotti et al., 2002; Lohrenz et al., 2003).

Finally, we found evidence that the seasonal relationship between nutrient availability and $a^*_{ph}(\lambda)$ could be extended to interannual scales. Hydrographic conditions, such as freshwater flow and nutrient loading, have been shown to impose interannual variability on the general pattern of phytoplankton succession in CB (Adolf et al., in preparation). The strong negative correlation we observed between $a^*_{ph}(443)$ and freshwater flow and in spring and summer (Fig. 7) suggests an approach to estimate $a^*_{ph}(\lambda)$ in CB on an interannual basis. We submit that predictions of floral composition based on freshwater flow and nutrient loading can be used to estimate seasonal and regional $a^*_{ph}(\lambda)$ and run SA models without the need for coincident bio-optical measurements. Freshwater discharge rates for the Susquehanna River and most rivers and streams in the United States are available from USGS. As our analysis of $a^*_{ph}(\lambda)$ indicated, most of the variability of $a^*_{ph}(\lambda)$ was associated with 'pigment packaging' that affects the magnitude of absorption, and not with 'pigment composition' that affects spectral shape. Thus, a constant spectral shape for $a^*_{ph}(\lambda)$ may be assumed for CB, and the magnitude of $a^*_{ph}(\lambda)$ at all wavelengths predicted from a relationship of $a^*_{ph}(443)$ to freshwater flow (Fig. 7). This relationship could be used to avoid the need to define abrupt seasonal transitions of $a^*_{ph}(\lambda)$ for parameterization of GSM01-CB, and to account for interannual variability of nutrient loading.

The use of regional mean S_{cdm} in GSM01-CB did not adequately represent the variability present in MAB. Variability of S_{cdm} can result from mixing of CDOM of biogenous origin, characterized by higher S values, with CDOM of terrigenous origin. The influence of terrigenous CDOM typically declines in shelf and slope waters (Blough et al., 1993; Nelson and Guarda, 1995; Vodecek et al., 1997; Blough and Del Vecchio, 2002; Rochelle-Newall and Fisher, 2002). Delivery of terrigenous CDOM to MAB in plumes of CB and DB is subject to meteorological forcing (Johnson et al., 2001) and, therefore, occurs in pulses. Biologically derived CDOM (Peacock et al., 1988; Carder et al., 1989) exhibits 'patchy' distributions common to phytoplankton. Variability of S_{cdm} may also result from photobleaching of CDOM during periods of prolonged stratification (Vodecek et al., 1997; Del Vecchio and Blough, 2002). Due to this combination of sources and sinks, the conservative relationship often observed in CB is not maintained in MAB. However, this trend of increasing S_{cdm} with distance offshore must be addressed in bio-optical modeling. Chomko et al. (2003) demonstrated the need for a variable S_{cdm} value in MAB to make their spectral optimization model agree with in situ data. We propose that the relationship between S_{cdm} and $a_{cdm}(443)$ found for MAB (Fig. 10b) could be incorporated into GSM01-CB through the use of an iterative process in which S_{cdm} is selected based on

model estimates of a_{cdm}. This modification to GSM01-CB would avoid the need to define abrupt regional boundaries for parameterization of S_{cdm} in MAB.

5. Conclusions

Local parameterization of GSM01 improved retrievals of chl *a* compared to both OC4v.4 and GSM01 in most regions, and GSM01-CB performed better than OC4v.4 overall. In addition, GSM01-CB returned reasonable estimates of $a_{cdm}(443)$. The modeling results indicated relatively high uncertainties for all model products, reflecting the difficulty of working in these bio-optically complex waters. We have suggested alternative approaches to parameterization of $a^*_{ph}(\lambda)$ and S_{cdm} that avoid reliance on space and time boundaries. GSM01-CB is also limited by poor parameterization of particle scattering. Field measurements are needed to determine the seasonal and regional variability in magnitude and spectral variability of b_b throughout CB/MAB. Despite these caveats, GSM01-CB products from currently-available SeaWiFS radiances were reasonable for chl *a* and $a_{cdm}(443)$ and captured large-scale regional and seasonal trends. Low and negative $L_{WN}(\lambda)$ from SeaWiFS resulted in the loss of chl *a* retrievals for up to 25% of CB, suggesting that improved atmospheric correction combined with an SA model would greatly benefit chl *a* retrievals for Case 2 waters. Results of this study should be considered a starting point from which to evaluate further improvements to SA models as more in situ data become available, and as improvements to atmospheric correction are developed and implemented.

Acknowledgments

The authors wish to thank Bill Boicourt, Kathleen Cone, Wayne Esaias, Ed Houde, Christy Jordan, Mike Lomas, Chuck McClain, Stephane Maritorena, Dave Miller, Mike Roman, the captains and crews of the RV *Aquarius* and *Cape Henlopen*, and the SeaWiFS/SeaDAS groups for their valuable contributions to this work. Support from NASA, NSF, EPA. NOAA, and Maryland Sea Grant are gratefully acknowledged. Contribution No. 3759 of Horn Point Laboratory, University of Maryland Center for Environmental Science.

References

Adolf, J.E., Harding Jr., L.W., Mallonee, M.E. Phytoplankton chemotaxonomic indicators and primary productivity in Chesapeake Bay, 1995–2000 (submitted for publication).

Austin, R.W., 1974. The remote sensing of spectral radiance from below the ocean surface. In: Jerlov, N.G., Nielson, E.S. (Eds.), Optical Aspects of Oceanography. Academic Press, San Diego, pp. 317–344.

Blough, N.V., Del Vecchio, R., 2002. Chromophoric dissolved organic matter (CDOM) in the coastal environment. In: Hansell, D., Carlson, C. (Eds.), Biogeochemistry of Marine Dissolved Organic Matter. Academic Press, San Diego, CA, pp. 509–546.

Blough, N.V., Zafirou, O.C., Bonilla, J., 1993. Optical absorption spectra of waters from the Orinoco River outflow: terrestrial input of colored organic matter to the Caribbean. Journal of Geophysical Research 98, 2271–2278.

Bricaud, A., Morel, A., Prieur, L., 1983. Optical efficiency factors of some phytoplankters. Limnology and Oceanography 28, 816–832.

Bricaud, A., Babin, M., Morel, A., Claustre, H., 1995. Variability in the chlorophyll-specific absorption coefficients of natural phytoplankton: analysis and parameterization. Journal of Geophysical Research 100, 13321–13332.

Carder, K.L., Steward, R.G., Harvey, G.R., Ortner, P.B., 1989. Marine humic and fulvic acids: their effects on remote sensing of ocean chlorophyll. Limnology and Oceanography 34, 68–81.

Carder, K.L., Chen, F.R., Lee, Z.P., Hawes, S.K., Kamykowski, D., 1999. Semianalytic Moderate-Resolution Imaging Spectrometer algorithms for chlorophyll a and absorption with bio-optical domains based on nitrate-depletion temperatures. Journal of Geophysical Research 104, 5403–5421.

Carder, K.L., Chen, F.R., Lee, Z.P., Hawes, S.K., Cannizzaro, J.P., 2003. MODIS Ocean Science Team Algorithm Theoretical Basis Document (ATBD 19) Case 2 Chlorophyll *a*.

Chomko, R.M., Gordon, H.R., Maritorena, S., Siegel, D.A., 2003. Simultaneous retrieval of oceanic and atmospheric parameters for ocean color imagery by spectral optimization: a validation. Remote Sensing of Environment 84, 208–220.

Ciotti, A.M., Lewis, M.R., Cullen, J.J., 2002. Assessment of the relationships between dominant cell size in natural phytoplankton communities and the spectral shape of the absorption coefficient. Limnology and Oceanography 47, 404–417.

Cleveland, J.S., 1995. Regional models for phytoplankton absorption as a function of chlorophyll *a* concentration. Journal of Geophysical Research 100, 13333–13344.

Del Vecchio, R., Blough, N.V., 2002. Photobleaching of chromophoric dissolved organic matter in natural waters: kinetics and modeling. Marine Chemistry 78, 231–253.

Duysens, L.N.M., 1956. The flattening of the absorption spectrum of suspensions as compared to that of solutions. Biochimica et Biophysica Acta 19, 1–12.

Fargion, G.S., Mueller, J.L., 2000. Ocean Optics Protocols for Satellite Ocean Color Sensor Validation, Revision 2. NASA Tech. Memo. 2000-209966. NASA Goddard Space Flight Center, Greenbelt, Maryland.

Fisher, T.R., Harding Jr., L.W., Stanley, D.W., Ward, L.G., 1988. Phytoplankton, nutrients and turbidity in the Chesapeake, Delaware and Hudson estuaries. Estuarine, Coastal and Shelf Science 82, 61–93.

Fisher, T.R., Peele, E.R., Ammerman, J.W., Harding Jr., L.W., 1992. Nutrient limitation of phytoplankton in Chesapeake Bay. Marine Ecology Progress Series 82, 51–63.

Garver, S.A., Siegel, D.A., 1997. Inherent optical property inversion of ocean color spectra and its biogeochemical interpretation 1. Time series from the Sargasso Sea. Journal of Geophysical Research 102, 18607–18625.

Gordon, H.R., Morel, A., 1983. Remote Assessment of Ocean Color for Interpretation of Satellite Visible Imagery: a Review. Springer-Verlag, New York.

Gordon, H.R., Ding, K., 1992. Self-shading of in-water optical instruments. Limnology and Oceanography 37, 491–500.

Gordon, H.R., Brown, O.B., Evans, R.H., Brown, J.W., Smith, R.C., Baker, K.S., Clark, D.K., 1988. A semianalytic radiance model of ocean color. Journal of Geophysical Research 93, 10909–10924.

Gould, R.W., Arnone, R.A., Martinolich, P.M., 1999. Spectral dependence of the scattering coefficient in case 1 and case 2 waters. Applied Optics 38, 2377–2383.

Green, S.A., Blough, N.V., 1994. Optical absorption and fluorescence properties of chromophoric dissolved organic matter in natural waters. Limnology and Oceanography 39, 1903–1916.

Harding Jr., L.W., Mallonee, M.E., Perry, E.S., 2002. Toward a predictive understanding of primary productivity in a temperate, partially stratified estuary. Estuarine, Coastal and Shelf Science 55, 437–463.

Harding Jr., L.W., Magnuson, A., Mallonee, M.E., 2004. Bio-optical and remote sensing observations in Chesapeake Bay. Estuarine, Coastal and Shelf Science, submitted for publication.

Johnson, D.R., Weidemann, A., Arnone, R., Davis, C.O., 2001. Chesapeake Bay outflow plume and coastal upwelling events: physical and optical properties. Journal of Geophysical Research 106, 11613–11662.

Jorgensen, P.V., 1999. Standard CZCS Case 1 algorithms in Danish coastal waters. International Journal of Remote Sensing 20, 1289–1301.

Kirk, J.T.O., 1975a. A theoretical analysis of the contribution of algal cells to the attenuation of light within natural waters. I. General treatment of suspensions pigmented cells. New Phytologist 75, 11–20.

Kirk, J.T.O., 1975b. A theoretical analysis of the contribution of algal cells to the attenuation of light within natural waters. II. Spherical cells. New Phytologist 75, 21–36.

Kirk, J.T.O., 1981. Estimation of the scattering coefficient of natural waters using underwater irradiance measurements. Australian Journal of Marine and Freshwater Research 32, 533–539.

Kirk, J.T.O., 1984. Dependence of the relationship between inherent and apparent optical properties of water on solar altitude. Limnology and Oceanography 29, 350–356.

Kirk, J.T.O., 1994. Characteristics of the light field in highly turbid waters: a Monte Carlo study. Limnology and Oceanography 39, 702–706.

Kishino, M., Takahashi, N., Okami, N., Ichimura, S., 1985. Estimation of the spectral absorption coefficient of phytoplankton in the sea. Bulletin of Marine Science 37, 634–642.

Lohrenz, S.E., Weidemann, A.D., Tuel, M., 2003. Phytoplankton spectral absorption as influenced by community size structure and pigment composition. Journal of Plankton Research 25, 35–61.

Mackey, M.D., Mackey, D.J., Higgin, H.W., Wright, S.W., 1996. CHEMTAX – a program for estimating class abundances from chemical markers: application to HPL measurements of phytoplankton. Marine Ecology Progress Series 144, 265–283.

Malone, T.C., 1992. Effects of water column processes on dissolved oxygen: nutrients, phytoplankton and zooplankton. In: Smith, D., Leffler, M., Mackiernan, G. (Eds.), Oxygen Dynamics in Chesapeake Bay: a Synthesis of Research. University of Maryland Sea Grant, College Park, Maryland, pp. 61–112.

Malone, T.C., Crocker, L.H., Pike, S.E., Wendler, B.W., 1988. Influences of river flow on the dynamics of phytoplankton production in a partially stratified estuary. Marine Ecology Progress Series 48, 235–249.

Malone, T.C., Ducklow, H.W., Peele, E.R., Pike, S.E., 1991. Picoplankton carbon flux in Chesapeake Bay. Marine Ecology Progress Series 78, 11–22.

Maritorena, S., Siegel, D.A., Peterson, A.R., 2002. Optimization of a semianalytical ocean color model for global-scale applications. Applied Optics 41, 2705–2714.

Marshall, H.G., Nesius, K.K., 1996. Phytoplankton composition in relation to primary production in Chesapeake Bay. Marine Biology 125, 611–617.

Mitchell, B.G., 1990. Algorithms for determining the absorption coefficient of aquatic particulates using the quantitative filter technique (QFT). SPIE Ocean Optics X 1302, 137–148.

Mitchell, B.G., Kahru, M., Weiland, J., Stramska, M., 2002. Determination of spectral absorption coefficients of particles, dissolved material and phytoplankton for discrete water samples. In: Mueller, J.L., Fargion, G.S. (Eds.), Ocean Optics Prorocols for Satellite Ocean Color Sensor Validation, Revision. NASA Tech. Memo. 2002-210004, vol. 2. NASA Goddard Space Flight Center, Greenbelt, MD, pp. 231–257.

Morel, A., 1988. Optical modeling of the upper ocean in relation to its biogenous matter content (Case 1 waters). Journal of Geophysical Research 93, 10749–10768.

Morel, A., Bricaud, A., 1981. Theoretical results concerning light absorption in a discrete medium, and application to specific absorption of phytoplankton. Deep-Sea Research 28, 1375–1393.

Morel, A., Gentili, B., 1991. Diffuse reflectance of oceanic waters: its dependence on sun angle as influenced by the molecular scattering contribution. Applied Optics 30, 4427–4438.

Morel, A., Gentili, B., 1993. Diffuse reflectance of oceanic waters. II. Bidirectional effects. Applied Optics 32, 6864–6879.

Nelson, J.R., Guarda, S., 1995. Particulate and dissolved spectral absorption on the continental shelf of the southeastern United States. Journal of Geophysical Research 100, 8715–8732.

Nelson, N.B., Siegel, D.A., Michaels, A.F., 1998. Seasonal dynamics of colored dissolved material in the Sargasso Sea (Part I). Deep-Sea Research 100, 8715–8732.

O'Reilly, J.E., Yoder, J.A., 2003. A comparison of SeaWiFS LAC Products from the Third and Fourth Reprocessing: Northeast US Ecosystem. In: Hooker, S.B., Firestone, E.R. (Eds.), Algorithm Updates for the Fourth SeaWiFS Data Reprocessing. NASA Tech. Memo. 2003-206892. NASA Goddard Space Flight Center, Greenbelt, MD, pp. 60–67.

O'Reilly, J.E., Maritorena, S., Mitchell, B.G., Siegel, D.A., Carder, K.L., Garver, S.A., Kahru, M., McClain, C.R., 1998. Ocean color algorithms for SeaWiFS. Journal of Geophysical Research 103, 24937–24953.

Parslow, J.S., Hoepffner, N., Doerffer, R., Campbell, J.W., Schlittenhardt, P., Sathyendranath, S., 2000. Case 2 ocean color applications. In: Sathyendranath, S. (Ed.), Remote Sensing of Ocean Colour in Coastal, and Other Optically-complex, Waters, Reports of the International Ocean-Colour Coordinating Group, No. 3. IOCCG, Dartmouth, Nova Scotia, Canada, pp. 93–114.

Peacock, T.P., Carder, K.L., Steward, R.G., 1988. Components of spectral attenuation for an offshore jet in the Coastal Transition Zone. Eos Transactions American Geophysical Union 69, 1125.

Petzold, T.J., 1972. Volume Scattering Functions for Selected Ocean Waters. Scripts Institute of Oceanography, La Jolla Scripts Institute of Oceanography Ref. 72–78.

Rochelle-Newall, E.J., Fisher, T.R., 2002. Chromophoric dissolved organic matter and dissolved organic carbon in Chesapeake Bay. Marine Chemistry 77, 23–41.

Roesler, C.S., Perry, M.J., 1995. In situ phytoplankton absorption, fluorescence emission, and particulate backscattering spectra determined from reflectance. Journal of Geophysical Research 100, 13279–13294.

Smith, R.C., Baker, K.S., 1981. Optical properties of the clearest natural waters (200–800 nm). Applied Optics 20, 177–184.

Smith, R.C., Baker, K.S., 1984. Analysis of ocean optical data. SPIE Ocean Optics VII 489, 119–126.

Smith, R.C., Baker, K.S., 1986. Analysis of ocean optical data. II. SPIE Ocean Optics VIII 637, 95–107.

Stramski, D., Kiefer, D.A., 1991. Light scattering by microorganisms in the open ocean. Progress in Oceanography 28, 343–383.

Stedmon, C.A., Markager, S., Kaas, H., 2000. Optical properties and signatures of chromophoric dissolved organic matter (CDOM) in Danish coastal waters. Estuarine, Coastal and Shelf Science 51, 267–278.

Sydor, M., Arnone, R.A., 1997. Effect of suspended particulate and dissolved organic matter on remote sensing of coastal and riverine waters. Applied Optics 36, 6905–6912.

Tzortziou, M., 2004. Measurements and characterization of optical properties in the Chesapeake Bay's estuarine waters using in situ measurements, MODIS satellite observations and radiative transfer modeling. Ph D dissertation, University of Maryland.

Van Heukelem, L., Lewitus, A.J., Kana, T.M., Craft, N.E., 1994. Improved separations of phytoplankton pigments using temperature-controlled high performance liquid chromatography. Marine Ecology Progress Series 114, 303–313.

Van Heukelem, L., Thomas, C.S., 2001. Computer-assisted high-performance liquid chromatography method development with applications to the isolation and analysis of phytoplankton pigments. Journal of Chromatography A 910, 31–49.

Vodecek, A., Blough, N.V., DeGrandpre, M.D., Peltzer, E.T., Nelson, R.K., 1997. Seasonal variation of CDOM and DOC in the Middle Atlantic Bight: terrestrial inputs and photooxidation. Limnology and Oceanography 42, 674–686.

Yentsch, C.S., Phinney, D.A., 1989. A bridge between ocean optics and microbial ecology. Limnology and Oceanography 34, 1694–1705.